Chem Soc Rev

REVIEW ARTICLE

View Article Online
View Journal | View Issue

Cite this: *Chem. Soc. Rev.*, 2016, **45**, 5985

Polypeptide self-assemblies: nanostructures and bioapplications

Chunhua Cai, Jiaping Lin,* Yingqing Lu, Qian Zhang and Liquan Wang

Received 7th January 2016

DOI: 10.1039/c6cs00013d

www.rsc.org/chemsocrev

Polypeptide copolymers can self-assemble into diverse aggregates. The morphology and structure of aggregates can be varied by changing molecular architectures, self-assembling conditions, and introducing secondary components such as polymers and nanoparticles. Polypeptide self-assemblies have gained significant attention because of their potential applications as delivery vehicles for therapeutic payloads and as additives in the biomimetic mineralization of inorganics. This review article provides an overview of recent advances in nanostructures and bioapplications related to polypeptide self-assemblies. We highlight recent contributions to developing strategies for the construction of polypeptide assemblies with increasing complexity and novel functionality that are suitable for bioapplications. The relationship between the structure and properties of the polypeptide aggregates is emphasized. Finally, we briefly outline our perspectives and discuss the challenges in the field.

1. Introduction

Over the past several decades, synthetic polypeptides, poly(amino acid)s, have received increasing attention in terms of controlled synthesis, structure–property relationships, and bio-related applications.[1–4] Polypeptide-based copolymers can self-assemble into diverse aggregate structures, such as spherical micelles, cylindrical micelles, vesicles, and hierarchical structures in selective solvents.[5–8] Due to their good biocompatibility, polypeptides and their assemblies are especially promising candidates as delivery systems for various therapeutic payloads, for example, drugs and DNA.[9–12] The hydrophilic shell stabilizes the aggregates in blood circulation, and the hydrophobic core acts as a nano-reservoir for therapeutic agents. In addition, mimicking the role of mineral proteins, polypeptide aggregates have been applied as modifiers to mediate the mineralization

Shanghai Key Laboratory of Advanced Polymeric Materials, State Key Laboratory of Bioreactor Engineering, Key Laboratory for Ultrafine Materials of Ministry of Education, School of Materials Science and Engineering, East China University of Science and Technology, Shanghai 200237, China. E-mail: jlin@ecust.edu.cn; Tel: +86-21-6425-3370

Chunhua Cai

Chunhua Cai received his BS degree (2004) and PhD degree (2010) under the supervision of Professor Jiaping Lin from East China University of Science and Technology (ECUST). Since then, he has worked in School of Materials Science and Engineering of ECUST. In 2016, he got a one-year term scholarship from Chinese Scholarship Council (CSC) and worked as a visiting scholar in Professor Stephen Z. D. Cheng's group at the University of Akron in the United States. His research focuses on the self-assembly of polypeptide-based copolymers.

Jiaping Lin

Jiaping Lin received his bachelor and master degrees from Shanghai Jiao Tong University, and PhD from East China University of Science and Technology (ECUST, 1993). Then, he obtained a postdoctoral fellowship from Japan Society for the Promotion of Science (JSPS), a Lise-Meitner fellowship of Fonds zur Förderung der wissenschaftlichen Forschung (FWF), and worked as a postdoctoral researcher in the Tokyo Institute of Technology and University of Linz in Austria, respectively. Returning home from abroad in 1997, he has been in ECUST ever since then. He became a full professor in 1999. His current research interests include macromolecular self-assembly, biomaterials and liquid crystalline polymers.

of inorganics in recent research.[13–15] For bio-related applications such as delivery vehicles and biomineralization additives, it is essential to control the morphology, structure, and functionality of polypeptide self-assemblies.

The molecular architecture is a basic factor determining the self-assembly behaviour of copolymers in solution.[16–20] Copolymers with various topologies, including block, graft, and dendrimer-like, display diverse self-assembly behaviours in selective solvents. However, synthesis of copolymers with various topologies and defined chemical compositions is a daunting task. The cooperative self-assembly of copolymers with secondary components, such as homopolymers, copolymers, nanoparticles (NPs), and small molecules, has therefore emerged as an appealing strategy for constructing various aggregates.[21–24] In addition, copolymer self-assembly behaviour is highly dependent on the preparation conditions such as the nature of the solvent and the polymer concentration. For the polypeptide-based copolymers, the ordering of polypeptide rods and the rod–coil chain conformation transition induce distinct self-assembly behaviours.[25–29] Furthermore, because polypeptides are chiral polymers, chirality should be another distinctive factor influencing the self-assembly behaviour and function of the formed structures.[30–32]

A high-performance delivery vehicle has various demands, such as stability during circulation, delivering payloads to specific sites, and releasing payloads in a desired manner.[33–35] Polypeptide assemblies are good candidates for "smart" delivery, responding to physical and chemical stimuli based on the following characteristics. (a) Ionic polypeptides such as poly(L-glutamic acid) (PLGA) and poly(L-lysine) (PLL) can be used to physically bind drugs bearing opposite charge. Changing the pH of the solution weakens the binding and releases the drugs. With the change of pH, the conformation of polypeptides may also change, facilitating the release of the drugs.[36–39] (b) Polypeptides contain various reactive groups, which could serve to chemically conjugate drugs with labile chemical bonds. The loaded drugs can be released by breaking the labile chemical bonds.[40–42] (c) Due to the physical or chemical stimuli, the structure of the deliveries can be disrupted, which induces a rapid release of payloads.[43,44]

Biominerals, generated under the mediation of natural proteins, have hierarchical organization and superior properties.[45–47] Inspired by protein-controlled mineralization, the biomimetic mineralization of inorganics in the presence of synthetic polymers has attracted increasing attention.[48,49] Due to the resemblance in chemical composition to that of proteins, the synthetic hydrophilic polypeptides such as PLGA, polyaspartic acid (PAsp), PLL and their derivatives have been used to mediate the mineralization of inorganics.[50–56] Later, it was found that polymer self-assemblies are suitable additives mediating the biomineralization of inorganics.[57,58] Because the polypeptide aggregates can mimic the folded structure of the mineral proteins, these polypeptide aggregates are more attractive for mediating the mineralization of inorganics.[59–64]

An experimental understanding of both the self-assembly behaviour of copolymers and the release behaviour of deliveries usually suffers from difficulties related to limited experimental techniques. However, theory and simulation can somewhat overcome the limitations because they provide more straightforward results and detailed information than pure experiments, including the chain distribution in the aggregates, the release process of the drugs, structural variation of delivery during drug release, and crystallization behaviour of biomineralization.[65–68]

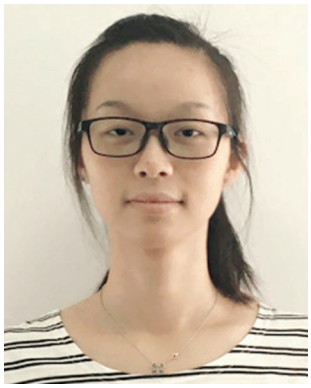

Yingqing Lu

Yingqing Lu was born in Hunan Province, China, in 1990. She received her Bachelor's degree in Polymer Materials and Engineering from East China University of Science and Technology (ECUST) in 2012. She is currently a doctoral candidate in Materials Science and Engineering at ECUST under the supervision of Professor Jiaping Lin, undertaking biomimetic mineralization and self-assembly of polypeptide-based copolymers.

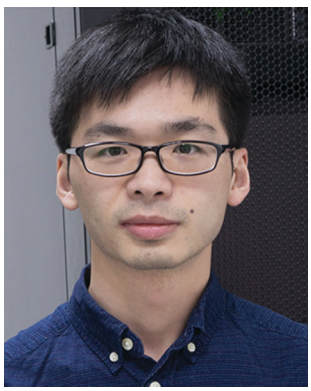

Qian Zhang

Qian Zhang was born in Jiangxi Province, China, in 1989. He received his Bachelor's degree in Polymer Materials and Engineering from East China University of Science and Technology (ECUST) in 2010. He is currently a doctoral candidate in Materials Science and Engineering at ECUST under the supervision of Professor Jiaping Lin, undertaking the theoretical simulations of self-assembly in polymeric systems.

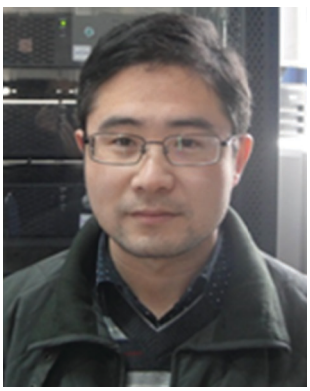

Liquan Wang

Liquan Wang was born in Zhejiang, China, in 1982. He received his PhD degree under the supervision of Professor Jiaping Lin in Materials Science and Engineering from ECUST in 2011. Now he is working as an associate professor in the School of Materials Science and Engineering of ECUST. His research interest is focused on the theoretical simulations of complex polymer systems.

To date, various simulation methods such as molecular dynamics (MD), dissipative particle dynamics (DPD), and Brownian dynamics (BD) simulations have been applied as powerful tools to investigate such behaviours.[69–75] The combination of experiments and simulation has many advantages.[76–82] Constructing valid simulation models to study polypeptide-based copolymers can not only support the experimental results but also give valuable information that could not be obtained from experiments.[20,27,28,79]

In this review, we summarize the state of the art in designing nanostructures of polypeptide self-assemblies and review the bio-related applications of polypeptide assemblies. This article is divided into three parts. The first part discusses the self-assembly behaviour of polypeptide-based copolymers. The ordered packing of rigid polypeptide segments that induces distinct self-assembly behaviours is reviewed in detail. In the second part, the recent advances in polypeptide assemblies serving as ''smart'' delivery systems are featured. Special attention has been paid to the stimuli-induced aggregate structural variation and stimuli-responsive release behaviour under various stimuli. In addition, the effect of the chirality of polypeptide building blocks on self-assembly behaviour, as well as the delivery and release behaviour of the vehicles, is emphasized in the first and second parts. The third part reviews biomimetic mineralization mediated by polypeptide-based aggregates. In particular, in each part we emphasize the importance of theoretical simulations in studies on polymer self-assembly, drug loading and delivery behaviours, and biomineralization behaviours.

2. Nanostructures of polypeptide-based self-assemblies

Polypeptide copolymers can self-assemble into diverse aggregate structures, including spherical micelles, cylindrical micelles, and vesicles. Moreover, hierarchical structures such as superhelices have also been observed in recent work.[5–8,83] The molecular architecture is a basic factor determining the self-assembly behaviour of polypeptide-based amphiphilic copolymers. With the development of polymer chemistry, copolymers with various topologies, including block, graft, brush-like, and dendrimer-like copolymers, have been synthesized. These copolymers display diverse self-assembly behaviours in selective solvents. In addition, cooperative self-assembly of polypeptide copolymers with secondary components has emerged as an appealing strategy to produce diverse aggregates with designed structures and functionalities.[21–24] A variety of guest components, including hydrophobic homopolymers,[84–87] amphiphilic copolymers,[88,89] nanoparticles (NPs),[90,91] and small molecules,[92] have been applied to cooperatively self-assemble with polypeptide copolymers.

Compared with conventional polymers, a distinguishing characteristic of polypeptides is that they can adopt various conformations, including random coil, α-helix, and β-sheet.[30–32] The conformation of the polypeptide determines the properties of chains, such as rigidity and solubility in solution, which further influences the self-assembly behaviour of the polypeptide copolymers. For example, poly(γ-benzyl L-glutamate) (PBLG) acts as a rigid rod in α-helix conformation; when adopting random coil conformation, PBLG becomes a flexible chain.[28] In aqueous solution, poly(L-glutamic acid) (PLGA) with a random coil conformation dissolves better than those with α-helix and β-sheet conformations.[30] Under certain conditions, the conformation of a polypeptide can transform from one to another, and the morphology and structure of the polypeptide assemblies can be varied by these transitions.[5,28,30–32] In addition, because polypeptides are chiral polymers, their chirality should be another important factor regulating the self-assembly behaviour of polypeptide copolymers. In this section, the self-assembly into various nanostructures of polypeptide copolymers and their corresponding mixtures are reviewed.

2.1 Aggregates self-assembled from single-component polypeptide copolymers

As elucidated by conventional block copolymer self-assembly systems, for example, polystyrene-*b*-poly(ethylene glycol) (PS-*b*-PEG), the morphology of the aggregates is mainly determined by the architecture and composition of the copolymers.[93–95] Preparation conditions such as the nature of the solvent and the polymer concentration also affect the aggregate morphology. For polypeptide copolymers, several distinct factors, including the ordering of rigid α-helical polypeptide chains, the variation of chain packing induced by conformation transitions, and the stimuli-induced solubility change of hydrophilic polypeptides, are applied to adjust the self-assembly behaviour of polypeptide copolymers. In the following content, we discuss the self-assembly behaviour of polypeptide copolymers with various macromolecular architectures.

2.1.1 Aggregates self-assembled from polypeptide block copolymers. Block copolymers are the most studied building units in constructing self-assemblies, and they usually serve as models to study the principles of polymer self-assembly. In recent years, the self-assembly of polypeptide block copolymers has attracted increasing attention.[5–8] For polypeptide copolymers containing rigid hydrophobic polypeptide segments, the ordered packing of polypeptide rods causes the copolymer to display distinct self-assembly behaviours.[25–29,96–99]

Recently, Lin *et al.* studied the self-assembly behaviour of PBLG-*b*-PEG-*b*-PBLG (BEB) triblock copolymers as a function of the PBLG block length and preparation conditions.[99] In the copolymer, PEG (degree of polymerization, DP, is 112) is hydrophilic and forms a corona around the aggregate core, whereas PBLG (DP is varied from 80 to 210) is hydrophobic and adopts a rigid α-helix conformation. They found that PBLG-*b*-PEG-*b*-PBLG triblock copolymers can self-assemble into vesicles when the PBLG block length is relatively short (BEB80, ''80'' indicates the DP of the PBLG blocks, Fig. 1a). Increasing the DP of the PBLG block from 80 to 150 and 210 induces a morphological transition from vesicles to spheres (Fig. 1a–c). In addition, as shown in Fig. 1d, when the initial polymer concentration increases, giant vesicles with diameters up to 2 μm can be produced. Such giant vesicles possess a larger hollow space and are promising in bioapplications such as drug delivery. Moreover, they applied dissipative particle dynamics

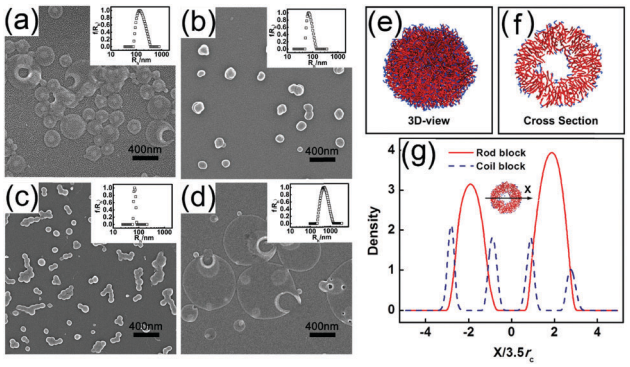

Fig. 1 (a–d) Typical SEM images of aggregates formed by: (a) BEB80, 0.5 g L^{-1}; (b) BEB150, 0.5 g L^{-1}; (c) BEB210, 0.5 g L^{-1}; and (d) BEB80, 1 g L^{-1}. Inset plots show the hydrodynamic radius distribution of aggregates in aqueous solution. (e–g) DPD simulations of the vesicle structure self-assembled from rod–coil–rod model triblock copolymers: (e) 3D-view of a vesicle; (f) cross-section of a vesicle; and (g) one-dimensional density profiles of rod and coil blocks along the x-arrow of the vesicle. Reprinted with permission from ref. 99. Copyright 2014 Elsevier B.V.

(DPD) simulations on model rod–coil–rod triblock copolymers to further study the structure of the vesicles. The simulation results are presented in Fig. 1e–g. It was revealed that the rod–coil–rod triblock copolymers self-assemble into vesicles and the rigid PBLG blocks align in parallel with each other to form the monolayer vesicle wall (Fig. 1e and f). In addition, the simulation provided more information that could not be obtained from the experiments, such as the chain distributions. As shown in Fig. 1g, the density profile of the PBLG rods contains a bimodal feature, whereas that of the PEG coils contains a tetramodal feature, which is a typical characteristic of the vesicles. These simulation results can further guide the experimental design of polypeptide self-assemblies. In a very recent work, He *et al.* prepared two-dimensional (2D) disk-like micelles with cylindrical pores self-assembled from PBLG-*b*-PEG diblock copolymers in solution.[29] The thickness of the disk is close to the calculated length of PBLG rods, which implies that the PBLG segments form the middle layer of the disk-like micelles and the PEG segments form shell layers. These two examples revealed that the rigidity of α-helical PBLG blocks played a key role in the self-assembly behaviours.

Water-soluble polypeptides such as PLL and PLGA can serve as hydrophilic segments in block copolymers, and the self-assembly behaviour is usually pH-sensitive because the solution pH determines the conformation and solubility of the hydrophilic polypeptides.[100–103] Monge and co-workers reported the synthesis and aggregation behaviour of poly(*N*,*N*-diethylacrylamide) (PDEAm)-*b*-PLL block copolymers.[103] The PDEAm-*b*-PLL was prepared by ring-opening polymerization (ROP) of N_ε-trifluoroacetyl-L-lysine *N*-carboxyanhydride (NCA) using terminated-thiol PDEAm as a macroinitiator. After deprotection of the amine groups of L-lysine, pH- and thermo-sensitive PDEAm-*b*-PLL block copolymers were obtained (PLL: pH-sensitive; PDEAm: thermo-sensitive). At pH 2 and 25 °C, both blocks are water-soluble, and no aggregates are formed. When the acidic solution is converted into basic solution, the solubility of PLL decreases, and micelles are formed with a PLL core and a PDEAm shell. At higher temperature (60 °C), rod-like (pH 2) or spherical (pH 10) aggregates always form with a PDEAm core and a PLL shell.

The conformation transition of core-forming polypeptides usually induces a morphological transformation of the polypeptide block copolymer aggregates.[28,104] In a recent work, Li *et al.* synthesized PEG-*b*-poly(γ-(2-methoxyethoxy)esteryl-L-glutamate) (PEG-*b*-P(EG_2LG)) diblock copolymers *via* ROP of EG_2LG NCA using PEG-NH_2 as a macroinitiator.[104] They observed a polypeptide conformation-induced aggregate morphological transition. In pristine aqueous solution, the P(EG_2LG) block adopts primarily α-helix conformation, and extension of the thermal annealing time drives the secondary structural transformation of the P(EG_2LG) block into a β-sheet. This polypeptide conformation change induces the transformation of the aggregate structure from wormlike micelles into nanoribbons.

Block copolymers are widely studied in self-assembly research. For polypeptide-based block copolymers, making use of the characteristics of the polypeptide segments, including the rigidity of the chain and conformation transition under certain conditions, has led to diverse self-assembly structures. In addition to these simple diblock and triblock copolymers, there have been few studies on the self-assembly of polypeptide-based multi-block copolymers. Multi-block copolymers, typically $(AB)_n$-type and $A(BC)_n$-type, display unique self-assembly behaviours that have been illustrated through experiments and simulations.[105–107] Polypeptide-based multi-block copolymers could generate new assembly features. For example, due to the inherent structural features of the polypeptide segments, these multi-block polypeptide block copolymers are promising materials for the construction of hierarchical structures with multiple sensitivities to their surroundings.

2.1.2 Aggregates self-assembled from polypeptide graft copolymers. Graft copolymers are another important class of building polymers that lead to aggregates with multiple morphologies.[16,108–112] Compared with block copolymers, graft copolymers have received less attention but have obvious advantages in adjusting the self-assembly behaviours by changing the side chain properties, such as the grafting density, chain length, and environmental sensitivity. In polypeptide graft copolymers, the polypeptide segments can serve as either backbones or side chains.[113–120]

Kuo *et al.* used a combination of ATRP, ROP, and click chemistry to synthesize polystyrene-*b*-poly(γ-propargyl-L-glutamate-*g*-ethylene oxide) (PS-*b*-(PPLG-*g*-MEO2)) block-graft copolymers.[117] The conformation of the PPLG polypeptide segments was confirmed to be an α-helix. Their self-assembly behaviour was studied by adding water (selective solvent) to the polymer solution in DMF (common solvent). As shown in Fig. 2a–f, the morphology of the aggregate was dependent on the water content. Increasing the water content caused the aggregate morphology transition from spherical micelles to long cylinders, vesicles, and large compound micelles. This process of aggregate morphological transition as a function of the water content is illustrated in Fig. 2g.

Upon study of the self-assembly of PBLG-*g*-PEG graft copolymers, Lin *et al.* observed a variety of aggregates, including

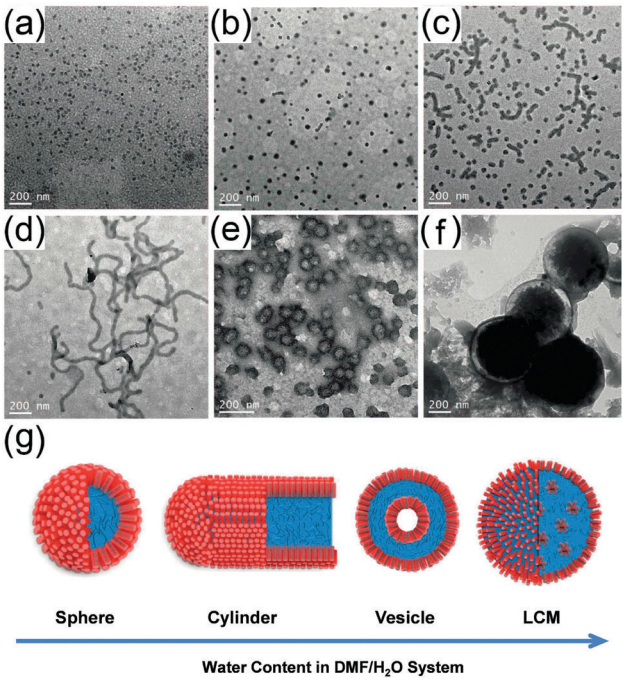

Fig. 2 (a–f) TEM images of the PS-*b*-(PPLG-*g*-MEO2) block-graft copolymer aggregates in DMF–water at water contents of (a) 1 wt%, (b) 1.5 wt%, (c) 2.5 wt%, (d) 4 wt%, (e) 4.5 wt%, and (f) 5.5 wt%. (g) Schematic representation of the morphological changes of the PS-*b*-(PPLG-*g*-MEO2) block-graft copolymer aggregates in the DMF–water system with increasing water content. Reproduced from ref. 117 with permission from The Royal Society of Chemistry.

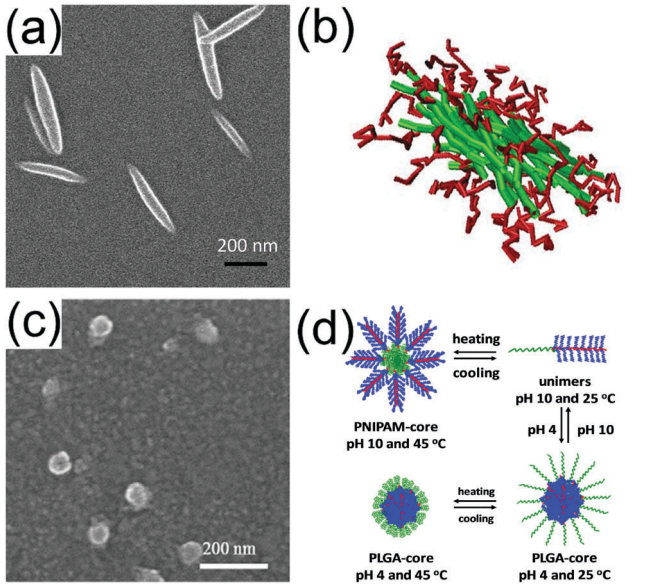

Fig. 3 (a and b) Spindle-like aggregates self-assembled from PBLG-*g*-PEG (rod-*g*-coil) graft copolymers: (a) SEM image and (b) DPD simulation predictions. (c and d) Thermo- and pH-responsive self-assembly behaviour of PNIPAM-*b*-(PGMA-*g*-PLGA) block-graft copolymers: (c) typical SEM images of micelles formed at pH 10 and 45 °C and (d) schematic illustration of thermo- and pH-responsive micellization. (a) Reprinted with permission from ref. 118. Copyright 2010 American Chemical Society. (c and d) Reprinted with permission from ref. 132. Copyright 2013 Elsevier B.V.

spheres, rods, spindles, vesicles, and large compound micelles (LCMs).[118–120] Various factors were investigated, including the molecular weight of the PBLG and PEG chains, the degree of grafting of the PEG chains, initial solvent nature, initial polymer concentration, and the rate of addition of the selective solvent. They discovered a first example of vesicles formed by graft copolymers bearing a rigid backbone.[118] Moreover, spindle-like micelles which have seldom been observed in other polymer systems were observed (Fig. 3a). The ordering of polypeptide segments along the long axis of the spindle should take response for the formation of spindles. Using DPD simulations, they studied the ordering behaviour of such rod-*g*-coil graft copolymers. As shown in Fig. 3b, the simulation results reveal that the rigid backbones of the spindle-like micelles are aligned along the long axis in a manner of nematic liquid crystals and the PEG chains spread out of the aggregates.

Once multiple polymer chains are grafted onto one polymer backbone, multi-graft copolymers are obtained. The multi-graft copolymers can possess multiple functions.[121,122] By sequentially grafting poly(*N*-isopropyl acrylamide) (PNIPAM) segments and 2-hydroxyethyl methacrylate (HEMA) units onto a PLGA backbone, Chen *et al.* synthesized a polypeptide-based multi-graft copolymer (PLGA-*g*-PNIPAM&HEMA).[123] In acidic solution, PLGA adopts an α-helix conformation, and a helix-to-coil conformation transition of the PLGA chain occurs at approximately pH 6.5. PLGA becomes more hydrophilic under basic conditions in the coil conformation. PNIPAM is a thermo-sensitive block that becomes hydrophobic at temperatures above the lower critical solution temperature (LCST, approximately 32 °C). The graft copolymers can fully dissolve in aqueous solution at lower temperature (for example, 25 °C) and neutral or alkaline pH. Because these graft copolymers contain both pH-sensitive PLGA segments and thermo-sensitive PNIPAM segments, their self-assembly behaviour is pH- and thermo-sensitive. For example, at pH 8.0 and 60 °C, they self-assemble into spherical micelles (approximate diameter of 45 nm) with PNIPAM cores and PLGA shells. Under acidic conditions (pH < 6), the self-assemblies become unstable due to the lower hydrophilicity of the PLGA chains. The HEMA units which were incorporated into the micelle core can polymerize with each other to crosslink the micelle cores, retaining the diameter of the micelles. The crosslinked micelles are still pH- and thermo-sensitive. For example, a thermo-induced volume decrease was observed by increasing the temperature, which is related to the shrinkage of the PNIPAM chains. When the pH was lowered from 6.0 to 5.0 at 27 °C, a dramatic increase in the particle size was observed, as detected by DLS testing. This phenomenon can be explained by the aggregation of micelles induced by the protonation and increased hydrophobicity of the PLGA chains.

When the side chains of graft copolymers are densely distributed on a polymer backbone, so called brush-like copolymers are obtained. Brush-like copolymers exhibit distinct assembly features.[124–127] There is some work regarding the synthesis and self-assembly behaviours of polypeptide-based brush-like copolymers.[128–132] For example, the self-assembly behaviour of brush–coil block copolymers can be adjusted

through the length of the brush segments.[128] Tang *et al.* reported the synthesis and self-assembly behaviour of a PNIPAM-*b*-(PGMA-*g*-PLGA) brush–coil copolymer (PGMA: poly(glycidyl methacrylate)).[132] PNIPAM-*b*-PGMA-EDA was first synthesized by sequential RAFT polymerization of *N*-isopropylacrylamide and glycidyl methacrylate and subsequent reaction with ethylenediamine (EDA). The PNIPAM-*b*-(PGMA-*g*-PBLG) brush–coil copolymer was then obtained by ROP of BLG-NCA with PNIPAM-*b*-PGMA-EDA as the macroinitiator. After deprotection of benzyl groups on PBLG, the PNIPAM-*b*-(PGMA-*g*-PLGA) brush–coil copolymer was finally obtained. The brush–coil copolymer dissolves well at pH 10 and room temperature. Increasing the solution temperature leads to the formation of PNIPAM-core micelles (Fig. 3c). For this brush–coil copolymer solution, introducing acid can induce polymer self-assembly into micelles with a PLGA core and a PNIPAM shell. The PNIPAM shell shrinks when the temperature of the micelle solution increases. This pH- and temperature-induced aggregate morphological transition is illustrated in Fig. 3d.

Compared with their block counterparts and conventional graft copolymers, the polypeptide graft copolymers exhibit some interesting self-assembly behaviours that mainly result from (1) the pH-sensitivity enabled by the hydrophilic polypeptides, (2) the ordered packing tendency of the hydrophobic polypeptides, and (3) the convenient control over the hydrophilic/hydrophobic balance of the copolymers that further affects the aggregate morphology. However, there has been limited work on the self-assembly behaviour of polypeptide-based graft copolymers, and several promising concepts are therefore worth pursuing. For example, a graft copolymer containing rigid hydrophobic polypeptide side chains and a hydrophilic backbone chain can self-assemble into aggregates with a rigid polypeptide core, and the rigidity of the core-forming polypeptide chains leaves the aggregate core with sufficient room to encapsulate various guest species, such as drugs. Furthermore, few studies have been directed towards the self-assembly of graft copolymers in which both the hydrophilic and hydrophobic segments are polypeptides. The self-assembly behaviour of this type of graft copolymer is expected to be associated with the features of both the hydrophilic and hydrophobic polypeptide segments. It is expected that polypeptide graft copolymers could display diverse self-assembly behaviours and have wide potential applications.

2.1.3 Aggregates self-assembled from polypeptide copolymers with complex topology. In addition to block and graft copolymers, polypeptide-based copolymers with complex topology, such as dendrimer-like and hyperbranched polymers have also been synthesized, and their self-assembly behaviours have been studied.[133,134] Dendrimer-like polymers are a special type of polymer in which multiple polymer chains are connected together from a concentric point (group).[135–137] Although hyperbranched polymers are highly branched polymers, they are a special form of dendritic polymers that have a random branch-on-branch topology.[138–140] These polypeptide-based copolymers with complex topology display unique self-assembly properties and multivalent characteristics.

As reported in a recent work by Chen *et al.*, PLL_{40}-*b*-D2-$(PLGA_{15})_4$ (D2 is the second generation of poly(amido amine)) dendrimer-like polypeptide block copolymers exhibit multiple pH-sensitive self-assembly behaviours.[137] The copolymers can self-assemble into PLGA-core aggregates at acidic pH and PLL-core aggregates at alkaline pH, which is accompanied by a coil-to-helix conformation transition of PLGA and PLL segments, respectively. Self-assembled aggregates with various morphologies, such as large compound micelles, worm-like micelles, large compound vesicles, simple vesicles, and rigid tubular structures, have been obtained by increasing the solution pH. Fig. 4 shows typical TEM and SEM images of the aggregates prepared at various pH values. More interestingly, hierarchical assembled fractal structures of PLL_{40}-*b*-D2-$(PLGA_{15})_4$ were observed during solvent evaporation at higher pH. Fig. 4g displays a scheme of the structural evolution of these self-assemblies as a function of solution pH.

Dong *et al.* reported the synthesis and self-assembly of hyperbranched poly(ε-benzyloxycarbonyl-L-lysine)-*block*-poly(ethylene oxide) (HPZLys-*b*-PEO).[140] The self-assembly behaviour of the hyperbranched copolymers was compared with a linear counterpart (PZLys-*b*-PEO). For the hyperbranched copolymers, HPZLys was synthesized through click polycondensation of an AB_2-type PZLys macromonomer with α-thiol and ω-alkyne terminal groups (the thiol is the A unit and each π bond in the

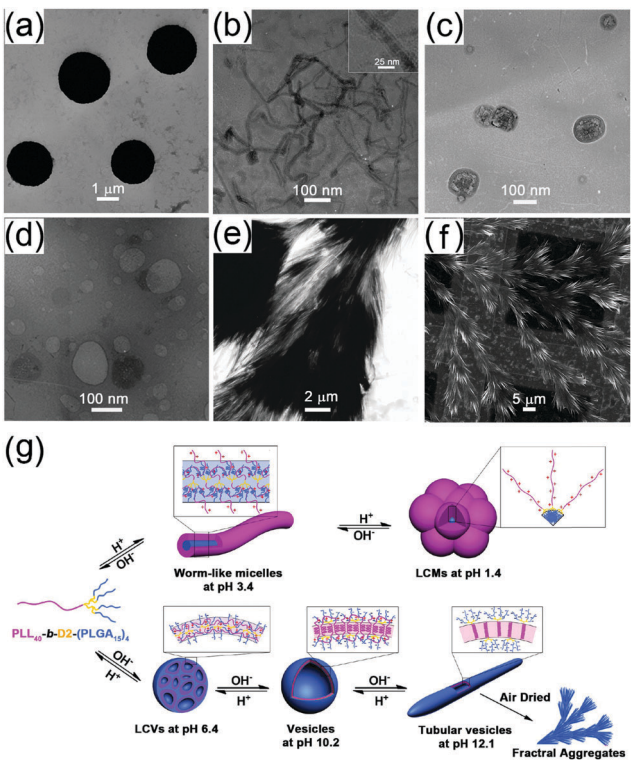

Fig. 4 (a–e) Typical TEM images of PLL_{40}-*b*-D2-$(PLGA_{15})_4$ aggregates in aqueous solutions: (a) pH 1.4, (b) pH 3.4, (c) pH 6.4, (d) pH 10.2, and (e) pH 12.1. (f) SEM image of aggregates at pH 12.1. (g) Schematic illustration of proposed pH-responsive "schizophrenic" aggregation behaviours of linear-dendron-like PLL_{40}-*b*-D2-$(PLGA_{15})_4$ in aqueous solution. Reprinted with permission from ref. 137. Copyright 2013 American Chemical Society.

alkyne is the B unit), and the resulting HPZLys was further conjugated with thiol-terminated PEO to generate the HPZLys-*b*-PEO block copolymer by consecutive thiol–yne chemistry. HPZLys and HPZLys-*b*-PEO mainly assume an α-helix conformation similar to their linear precursors. The self-assemblies of these copolymers were prepared by using DMF as the common solvent and water as selective solvent. HPZLys-*b*-PEO copolymers self-assemble into spherical micelles in aqueous solution. Compared with their linear counterpart of PZLys-*b*-PEO, HPZLys-*b*-PEO displays a much lower critical aggregation concentration, which demonstrates a dendritic topology effect.

Because of their unusual topological structure, polypeptide-based copolymers with complex topologies exhibit interesting self-assembly behaviours. Many peptide- or polypeptide-containing biomacromolecules, for example, collagen and glycoproteins, bear complex topologies, such as dendrimer-like and hyperbranched.[141,142] The knowledge obtained from self-assembly research on synthetic polypeptide-based copolymers with complex topologies is helpful for understanding the assembled structures and functionalities of polypeptide-containing biomacromolecules. In addition, because they mimic the molecular and assembly structures of peptide-containing biomacromolecules, these synthetic polypeptide-based copolymers with complex topologies have potential in bio-related applications, including tissue engineering and drug delivery. Therefore, self-assembly research on synthetic polypeptides with various complex topologies provides an important model for understanding the relationship between the structure and properties of peptide-containing biomacromolecules.

2.2 Aggregates self-assembled from polypeptide copolymer mixtures

Self-assembly of single-component copolymers, typically block copolymers, has been studied extensively, which provides opportunities for the construction of various nanostructures. However, the synthesis of copolymers with defined topologies and compositions is difficult. In recent work, the cooperative self-assembly behaviour of copolymers with a secondary hydrophobic component, such as homopolymers and NPs, has been studied through both experiments and simulations, and a variety of interesting nanostructures have been observed. In addition, for chiral polymers, introducing polymers with different chirality is another working strategy to regulate the self-assembly behaviours.[30–32] In this part, research on the control of the self-assembly structure of polypeptide copolymers through the introduction of a secondary component is featured.

2.2.1 Cooperative self-assembly of polypeptide copolymers with homopolymers. Bearing in mind that hydrophobic/hydrophilic balance is the most important factor determining the assembly structure, it is easy to envision the addition of hydrophobic core-forming polymers to adjust the aggregate morphology.[143–147] In fact, adding core-forming homopolymers is effective in modifying the morphology of aggregates formed by block copolymers. The molecular weight of the homopolymer is usually smaller than or approximate to that of the core-forming blocks. The morphological transition of block copolymer assemblies, for example, from vesicles to spherical micelles or from cylindrical micelles to vesicles has been observed by adding core-forming homopolymers.[143] For polypeptide-based copolymers, the effect of hydrophobic homopolymers on their self-assembly behaviours has not been well documented.[84–87] In this subsection, the effect of hydrophobic homopolymers on the self-assembly behaviour of polypeptide copolymers is reviewed, and typical examples are introduced in detail.

Recently, Cai *et al.* reported that right-handed superhelical fibres and rings with uniform diameters and screw-pitch sizes are formed from a binary system consisting of a rod–coil block copolymer of PBLG-*b*-PEG and a rigid homopolymer of PBLG.[86,87,148] Fig. 5a–c show TEM, SEM, and AFM images of the superhelices. Note that the molecular weight of the PBLG homopolymers is much larger than that of the PBLG-*b*-PEG block copolymers (more than 10 times). The high molecular weight of the PBLG homopolymer is crucial for the construction of the fibre-like structures. When the mixture systems contain low molecular weight PBLG homopolymers, they form spheres or spindles rather than superhelices. For example, in a work by Ponchel *et al.* on similar PBLG-*b*-PEG/PBLG mixtures in which the molecular weight of the PBLG homopolymers is comparable

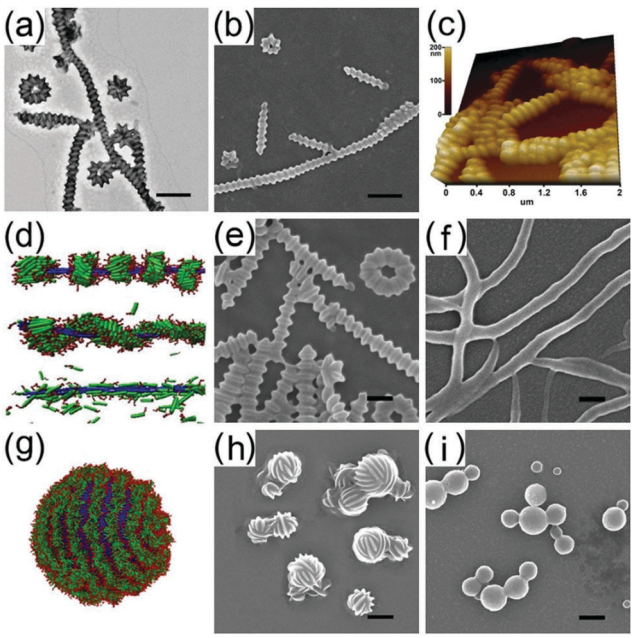

Fig. 5 (a–c) Morphology of superhelices prepared from PBLG-*b*-PEG/PBLG mixtures at 20 °C: (a) HRTEM, (b) SEM, and (c) AFM images. (d) Simulation predictions for hierarchical structures self-assembled from rod–coil block copolymers and rigid homopolymers with various levels of attraction between the rod/rod blocks (ε_{rr} = 2.4, 2.1, and 1.6, respectively, from up to down). (e) SEM image of abacus-like structures self-assembled from PBLG-*b*-PEG/PBLG mixtures at 40 °C. (f) SEM image of plain fibres self-assembled from PBLG-*b*-PEG/PBLG mixtures at 5 °C. (g) Simulation prediction of wool-ball-like structures formed by rod–coil block copolymers and coil homopolymers. (h) SEM image of wool-ball-like structures self-assembled from PBLG-*b*-PEG/PS mixtures at 40 °C. (i) SEM image of plain balls self-assembled from PBLG-*b*-PEG/PS mixtures at 5 °C. Scale bars: 500 nm for a, b, h, and i; 200 nm for e and f. Reprinted with permission from ref. 87. Copyright 2013 Wiley-VCH.

to that of the PBLG-*b*-PEG block copolymers, ellipsoidal particles with diameters less than 100 nm were obtained from mixtures with various weight ratios of block copolymers to homopolymers.[85]

The helix is one of the most fundamental geometrical shapes in nature and can be observed at all length scales: from the structure of DNA to a planetary helix nebula.[149–152] For example, tobacco mosaic virus (TMV) has a type of core–shell superhelix that contains an RNA core and coating proteins that assemble into a capsid with right-handed chirality.[153,154] In PBLG-*b*-PEG/PBLG superhelix systems, many possible interactions, including hydrophobic and dipolar π–π interactions, and the ordered packing tendency of the α-helical polypeptide rods are believed to be responsible for the formation of superhelical structures. However, understanding exactly how the observed structures are formed is a daunting task. To meet this challenge, Cai *et al.* carried out a Brownian dynamics (BD) simulation on a model rod–coil block copolymer/rigid homopolymer binary system to study the complex structure and the formation process.[87,148] As shown in Fig. 5d, the simulation results revealed that the homopolymers and block copolymers formed ordered structures. The rod–coil block copolymer can coat rod homopolymer bundles, and changing the level of attraction (ε_{rr}) between rod and rod blocks can result in different hierarchical structures. Three distinctive hierarchical morphologies, including abacus-like structures, superhelices, and plain fibres, were observed by decreasing the ε_{rr} from 2.4 to 2.1 and 1.6 (Fig. 5d). Under the guidance of the simulation predictions, they further designed a set of experiments on the PBLG-*b*-PEG/PBLG pair to experimentally explore the effect of attraction between rigid PBLG blocks on the structure of the formed assemblies. The regulation of attraction between the PBLG blocks is realized through the temperature of the experiment. Higher temperature corresponds to a stronger attraction between PBLG/PBLG pairs. Abacus-like structures are obtained at 40 °C (Fig. 5e). As shown in Fig. 5f, decreasing the temperature to 5 °C gives rise to the formation of plain fibres. These experimental results are in good agreement with the simulation predictions.

Furthermore, the rigid PBLG homopolymers were replaced with relatively flexible PS homopolymers to explore the importance of the guest homopolymers in the self-assembly behaviour of block copolymer/homopolymer mixtures.[87] A novel wool-ball-like structure was observed from PBLG-*b*-PEG/PS binary systems. The simulation results shown in Fig. 5g reveal that flexible homopolymers form large spherical aggregates and rod–coil block copolymers aggregate on the surface of the homopolymer sphere to form strips, in which the manner of the ordered packing is similar to that in the superhelices formed by rod–coil block copolymer/rigid homopolymer systems. The corresponding result from an experiment carried out at 40 °C is presented in Fig. 5h. With decreasing temperature, smooth spheres are formed due to the random packing of the PBLG-*b*-PEG block copolymers (Fig. 5i). In addition, they also studied the self-assembly behaviour of PS-*b*-PEG/PBLG binary systems, wherein a mixture of smooth fibres and spherical micelles was observed. For this system, the smooth fibres are formed by coating PS-*b*-PEG block copolymers on the rigid PBLG homopolymer bundles, while spherical micelles are formed from pure PS-*b*-PEG block copolymers. This set of experiments stresses the importance of the rigidity of the polymer blocks on the formation of the hierarchical structure.

In another recent work, using a combination of experiments and computer simulations, Chen and Lin *et al.* investigated the self-assembly behaviour of polyacrylic acid (PAA)-*g*-PBLG in the presence of high-molecular-weight PBLG homopolymers.[155] The aggregate morphologies of the mixture systems were dependent on the weight fraction of the PBLG homopolymers. Short rod-like micelles form with a lower weight fraction of PBLG homopolymers, whereas toroidal micelles appear with a higher weight fraction of PBLG homopolymers. Studies on the effect of the added water content on the toroid formation process revealed that rods and curved rods appear sequentially before the formation of toroids. Toroid formation *via* end-to-end connection of rods/cylinders is a common route.[124] They also performed DPD simulations to verify the structural transition as a function of the weight content of rigid homopolymers in the mixtures and to explore the formation mechanism of the toroidal aggregates. As predicted by DPD simulations, when the weight content of rigid homopolymers in the mixtures was lower, curved rod-like micelles appeared. Increasing the weight content of rigid homopolymers increased the length of the curved rod-like micelles, and toroidal micelles were formed by the end-to-end connection of curved rods. These simulation results reproduced the general features of the morphological transition of PAA-*g*-PBLG/PBLG mixtures as a function of the PBLG homopolymer content observed experimentally. In addition, the simulations showed that the rigid PBLG homopolymers prefer to locate in the centre of the interior core of the curved rod-like micelles and toroids. Moreover, they can provide information on the dynamic process for the formation of complex aggregates, which is difficult to attain through experiments.

The above-mentioned works demonstrate that the hydrophobic homopolymers can serve as templates for assembling amphiphilic block and graft copolymers. The structures of the self-assembled aggregates are determined by the characteristics of both homopolymers and copolymers. For example, depending on the rigidity degree (rigid or flexible), the homopolymers can act as either a fibre-like template or a spherical template, which determines the overall structure of the final aggregates. Furthermore, as inspired by the work stated above, some other available shaped materials such as multiwalled carbon nanotubes (MWCNTs) and crosslinked polystyrene spheres could serve as simple and effective templates.[156,157] Polypeptide copolymers can cover the template and generate patterned structures on the surface of templates through ordering of the rigid polypeptide blocks of copolymers. Due to the diverse ordering behaviours of polypeptide rods, various structures with different surface patterns could be produced. This should be an attractive topic in the future.

2.2.2 Cooperative self-assembly of polypeptide copolymers with copolymers. Similar to the self-assembly strategy for copolymer/homopolymer mixtures, cooperative self-assembly

of two copolymers is a promising way to obtain aggregates with controlled morphologies and structures.[158–161] In the past few years, there have been some examples of the self-assembly behaviour of polypeptide-based copolymer/copolymer mixtures, and interesting self-assembly phenomena have been observed.[88,89,162–164] Various interactions, including hydrophobic attractions between hydrophobic polypeptides, electrostatic attractions between oppositely charged polypeptides, and special interactions between polypeptides of different chiralities, are associated with the self-assembly behaviours of polypeptide copolymers/copolymers.

In a recent work reported by Zhuang *et al.*, polypeptide block copolymers were introduced to cooperatively self-assemble with polypeptide graft copolymers.[162] Both graft and block copolymers are constructed from PBLG and PEG segments, *i.e.*, PBLG-*g*-PEG graft copolymers and PBLG-*b*-PEG block copolymers. Pure graft copolymers self-assembled into vesicles, and pure block copolymers formed spherical micelles or vesicles. Fig. 6a and b show the vesicle morphology self-assembled from pure graft and block copolymers, respectively, while cylindrical hybrid micelles are formed for the graft/block copolymer mixtures (Fig. 6c). As revealed in their work, the pure graft copolymer vesicles are evoluted from primarily formed short cylinders. Therefore, for the graft/block copolymer mixtures, the block copolymers should prevent such a cylinder–vesicle morphology transition of the graft copolymers. They further performed self-consistent field theory (SCFT) simulations on this self-assembly system to explain such interesting self-assembly phenomena. The simulation results reproduced the morphological transitions observed in the experiments. As shown in Fig. 6d and e, the density profiles of the block and graft copolymers along the long and short axes of the hybrid cylindrical micelles indicate that the block copolymers are mainly located at the ends of the cylinders, which prevents the fusion of primary self-assembled cylinders into vesicles.

Kataoka and co-workers prepared a core–shell supramolecular assembly from PEG-*b*-PLL and PEG-*b*-PAsp polypeptide-based block copolymers.[163] These two block copolymers are oppositely charged: the PLL block is positively charged, and the PAsp block is negatively charged. It was found that polyion complex (PIC) micelles could be formed when the DP of the PLL and PAsp blocks was the same. However, the system with unmatched polymer length pairs could not form PIC micelles but only charge-neutralized polyion complexes, which are less stable than those formed from matched pairs. The key assumption by the authors is that the ion pairs have a uniform distribution in the core of PIC micelles.

Kimura *et al.* studied the self-assembly behaviour of a binary mixture containing polypeptide copolymers with opposite chirality of the polypeptide blocks.[164] These two polypeptide copolymers are $PSar_{25}$-*b*-P(L-Leu-Aib)$_6$ (SLL) and $PSar_{25}$-*b*-P(D-Leu-Aib)$_6$ (SDL). In these copolymers, the PSar block is a hydrophilic polypeptide and adopts a random coil conformation. P(L-Leu-Aib) and P(D-Leu-Aib) are core-forming hydrophobic polypeptides and adopt left- and right-handed α-helix conformations, respectively (Fig. 7a). The self-assembly behaviour of the mixtures was studied at 90 °C in Tris-HCl buffer solution (pH 7.4). As shown in Fig. 7b and f, pure SLL and SDL self-assembled into nanotubes. Mixtures of SLL and SDL with compositions of 20/80 or 80/20 (w/w) self-assembled into nano-sized round-bottom flasks (Fig. 7c and e), and a mixture with equal weights of SLL and SDL (50/50 w/w) formed vesicles (Fig. 7d). They explained these unique self-assembly processes as a stereo-complex formation of the helical amphiphiles. When SLL and SDL were mixed at 20/80 or 80/20, they were phase-separated into the pure component domain and the 1/1 stereo-complex

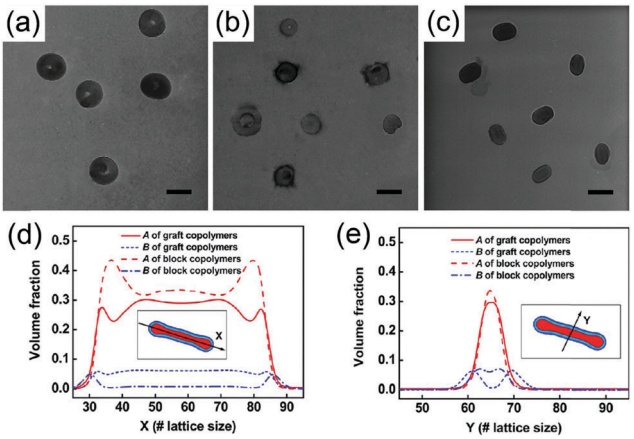

Fig. 6 (a–c) TEM images of aggregates self-assembled from (a) PBLG-*g*-PEG graft copolymers, (b) PBLG-*b*-PEG block copolymers, and (c) graft and block copolymer mixtures (mixture ratio 1 : 1 in weight). The scale bars represent 300 nm. (d and e) Density profiles of hydrophobic and hydrophilic blocks of the aggregates along the arrow in the inset for the cylindrical hybrid micelles. The insets show the two-dimensional distribution of the hydrophobic A blocks (presented as red) and hydrophilic B blocks (presented as blue). Reprinted with permission from ref. 162. Copyright 2012 American Chemical Society.

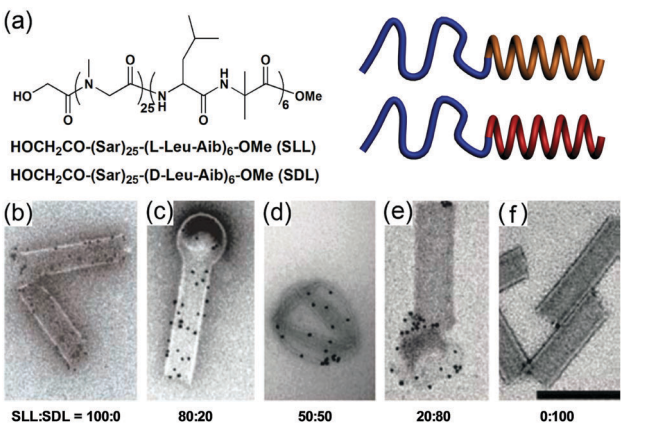

Fig. 7 (a) Molecular structures and schematic illustration of the polypeptide copolymers with right-handed helical blocks (SLL) and left-handed helical blocks (SDL). (b–f) Aggregate morphology of the SLL and SDL mixtures with various SLL/SDL weight ratios: (b) 100/0, (c) 80/20, (d) 50/50, (e) 20/80, and (f) 0/100. The dark dots are gold nanoparticles (10 nm) added to assemblies on the TEM grid. Scale bar is 200 nm. Reproduced from ref. 164 with permission from The Royal Society of Chemistry.

domain to yield the round-bottom flask morphology, which is a combined morphology of a nanotube and a vesicle.

For the polypeptide copolymer/copolymer mixtures, the polypeptide aggregates can be designed with various structures. The self-assembly behaviour is closely related to the mixture ratio of the two copolymers. Due to the various characteristics of the polypeptide segments, such as the rigidity and charge of the chain, the polypeptide-based copolymer/copolymer mixtures display diverse self-assembly behaviours. Furthermore, unique self-assembly behaviours can be observed for the mixtures containing two polypeptide copolymers with opposite chirality, which provides a new way to design the structure and function of self-assemblies. The cooperative self-assembly of two amphiphilic copolymers is a promising strategy to obtain aggregates with controllable morphologies and structures, which is significant for applications in the biomedical field and for functional materials.

2.2.3 Cooperative self-assembly of polypeptide copolymers with nanoparticles. Recently, polymer micelles have been used as templates to control the organization of nanoparticles.[165–168] Micelles can significantly enhance the stability of the dispersed state of nanoparticles in solution, which may facilitate their applications in catalysis, semiconductors, photonics, and biomimetic materials. Meanwhile, upon encapsulation of NPs, dramatic structural variation of aggregates is usually observed. For example, a transition between micelles and vesicles has been observed in conventional PS-*b*-PAA block copolymers and AuNP mixtures.[167] The effect of nanoparticles on the self-assembly behaviour of coil–coil block copolymers has been studied through experiments and theoretical simulations. Zhang *et al.* used SCFT simulation to study the effect of nanoparticles on the self-assembly behaviour of block copolymers.[168] It was shown that the aggregate morphology changes from vesicles to a mixture of spheres and cylinders by increasing the particle radius and particle volume fraction. The predictions are well in agreement with the existing experiments. However, there are few examples of the effect of nanoparticles on the self-assembly behaviour of polypeptide-based copolymers.[90,91] Polypeptide chains usually adopt a rigid α-helix conformation and prefer to adopt an ordered packing mode in the self-assembly process.[96] Introducing NPs can destroy the local ordering of polypeptide blocks, which further influences the self-assembly behaviour of the rod–coil polypeptide-based copolymers. Furthermore, the rigidity of polypeptide rods could induce a unique distribution of NPs.

Cai and co-workers reported that physically introduced AuNPs have a significant effect on the self-assembly behaviour of rod–coil PBLG-*b*-PEG block copolymers (Fig. 8a–c).[169] As shown in Fig. 8a, pure block copolymers self-assemble into long cylindrical micelles in which the PBLG blocks are orderly packed in the core. With the introduction of AuNPs, spherical micelles are obtained (Fig. 8b). Breakage of the ordered packing of PBLG rods induced by the added AuNPs takes responsibility for this type of morphological transition. They also performed a DPD simulation of the self-assembly of a model rod–coil block copolymer/nanoparticle mixture, which reproduced the experimental findings well. In addition, the order parameters of the rod blocks obtained from the simulations reveal that the ordered packing of rod blocks (PBLG block) in the micelle core was gradually destroyed by the incorporation of NPs. As shown in Fig. 8c, the order parameter of the rod block gradually decreases from approximately 0.8 for cylinders to nearly zero for spherical micelles. In another recent work, the same group further reported on the effect of AuNPs on the self-assembly behaviour of PBLG-*b*-PEG-*b*-PBLG triblock copolymers in aqueous solution.[170] A morphological transition from spindle-like micelles to vesicles was observed when a small portion of AuNPs was added. The AuNPs were located in the vesicle walls. The main reason for the transition of the aggregate morphology is believed to be the weakening of the interchain attraction between the rigid PBLG blocks caused by nanoparticle-induced disordering of the PBLG chains. These studies provide an effective method for controlling the aggregate morphology of polypeptide-based rod–coil copolymers.

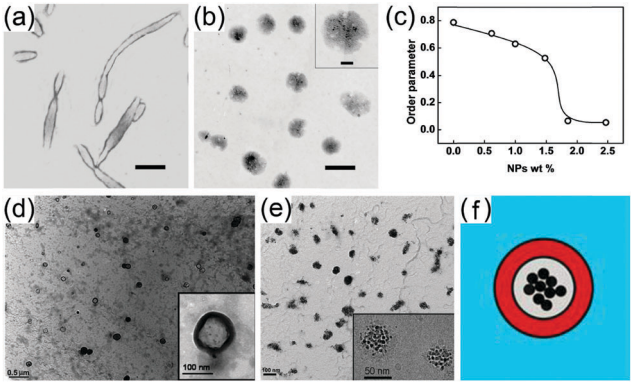

Fig. 8 (a–c) AuNP-induced cylinder–sphere morphological transition of PBLG-*b*-PEG block copolymer aggregates: (a) TEM image of cylindrical micelles self-assembled from PBLG-*b*-PEG block copolymers, (b) SEM image of spherical micelles prepared from PBLG-*b*-PEG/AuNP mixtures, and (c) order parameter of the PBLG blocks as a function of the nanoparticle concentration. Scale bars in (a) and (b) represent 250 nm. (d–f) Morphological transition from vesicles to spherical micelles of DMAEMA-*b*-PBLG block copolymer aggregates by adding γ-Fe_2O_3 nanoparticles: (d) TEM image of vesicles self-assembled from PDMAEMA-*b*-PBLG copolymers, (e) TEM image of micelles self-assembled from PDMAEMA-*b*-PBLG/γ-Fe_2O_3 mixtures, and (f) representation of the structure of the micelles with γ-Fe_2O_3 (in black) packed in the PBLG hydrophobic cores (in grey) wrapped by a hydrated PDMAEMA shell. (a–c) Reprinted with permission from ref. 169. Copyright 2012 American Chemical Society. (d–f) Reproduced from ref. 171 with permission from The Royal Society of Chemistry.

Lecommandoux *et al.* reported the cooperative self-assembly behaviour of amphiphilic poly(2-(dimethylamino)ethyl methacrylate) (PDMAEMA)-*b*-PBLG block copolymers and quasi-spherical iron oxide nanoparticles (γ-Fe_2O_3).[171] The PDMAEMA-*b*-PBLG block copolymers tended to form vesicles in solution, and the self-assembly behaviour of the block copolymer was pH- and temperature-responsive. A morphological transition from vesicles to micelles was observed by introducing γ-Fe_2O_3 nanoparticles, and the nanoparticles were observed to disperse within the hydrophobic PBLG domains. Fig. 8d and e show the TEM images of the vesicles (self-assembled from copolymers) and the micelles (self-assembled from copolymer/nanoparticle mixtures), respectively.

The structure of the micelles self-assembled from the PDMAEMA-*b*-PBLG copolymer/γ-Fe_2O_3 mixture is represented in Fig. 8f. The morphological transition is caused by the microphase separation between nanoparticles and PBLG chains, which is induced by a decreased attraction of the nanoparticles. This example demonstrates that the self-assembled structure of block copolymer/nanoparticle mixtures is governed not only by the amphiphilicity of the copolymers but also by excluded-volume interactions, which could be helpful in controlling the distribution of NPs in polypeptide aggregates.

Nanoparticles are effective additives used to induce a morphological transition of copolymer self-assemblies. For polypeptide copolymers containing rigid polypeptide segments (in α-helix conformation), the morphological transition of the aggregate is usually accompanied by disarrangement of the ordering of the polypeptide chains in the aggregate core. Most of the nanoparticles used are spherical and relatively small in size (less than 20 nm in diameter). When mixed with larger nanoparticles, which could serve as templates for polypeptide self-assembly, polypeptide copolymers may display different self-assembly behaviours. Furthermore, the effect of certain novel types of nanoparticles, such as rod-like and Janus nanoparticles, on the self-assembly behaviour of polypeptide copolymers has not been well studied. Polypeptide copolymer-based mixture systems containing non-classical nanoparticles could result in interesting self-assembly behaviours.

As demonstrated by the above-mentioned works, theoretical simulation is a powerful tool to investigate both the structure and the formation mechanism of polypeptide self-assemblies. Since the molecular weight of polypeptides is usually relatively high, coarse-gained models have usually been applied in the present simulation studies. However, the current coarse-gained simulations are limited in representing some certain fine structures of polypeptides, such as the chirality of polypeptide chains. Cai *et al.* recently found that the chirality of superhelices self-assembled from the PBLG-*b*-PEG/PBLG binary system can be controlled by experimental conditions such as the temperature and initial solvent nature.[172] Such a chirality transition is related to both the chirality of the PBLG backbone and the arrangement of side phenyl groups. However, this phenomenon is difficult to be simulated by the general coarse-grained models where the polypeptides are treated as rods. New strategies are thus necessary to simulate complex structures and obtain detailed information of polypeptide assemblies. All-atom simulation can successfully present the effect of the chirality of low-molecular-weight peptides on self-assembly behaviours. For example, using the all-atom simulations, Stupp *et al.* studied the self-assembly behaviours of peptide amphiphile (PA) molecules.[173,174] The packing manners of β-sheets in different PA aggregates (*e.g.*, stacks of β-sheets, spherical micelles, and cylindrical fibers) are revealed. The simulated structures are consistent with the experimental observations.

Although the all-atom simulations show some advantages in getting information regarding the chain conformation such as chirality, they still have difficulties in dealing with high-molecular-weight polypeptide systems, because of the unendurable computational cost in simulations. One way to solve this problem is to further develop the coarse-grained models by considering the information at the molecular level. For example, Grason *et al.* developed a new coarse-grained simulation method, which combines the Frank elastic energy with SCFT. They used this method to investigate the self-assembly behaviours of chiral block copolymers in the bulk phase. The simulation successfully reproduced experimental results, which indicates that this novel simulation approach can be useful in studying chiral block copolymers.[175,176] In addition, as revealed by Terentjev *et al.*, introducing bond angle and dihedral potential to the coarse-grained molecular model can present the rigidity structure information of the polypeptides in simulations.[177] Using the coarse-grained BD simulation method, they simulated a transformation between an expanded random coil and a dense helical or a globular state of single polypeptide chains. Therefore, it is possible to develop suitable simulation methods based on the coarse-grained model to simulate the self-assembly behaviour of polypeptide copolymers, which could be able to cover both the chirality and the rigidity structure feature of polypeptide chains. These developed simulations should be able to reproduce interesting experimental phenomena, such as the handedness of superhelices self-assembled from PBLG-*b*-PEG/PBLG binary systems, which can further guide experimental research.

3. Polypeptide assemblies serve as delivery vehicles

In the past two decades, polymer micelles have been comprehensively investigated as carriers to deliver various therapeutic payloads.[178–180] Polymer micelles are similar in size and structure to natural carriers of viruses and serum lipoproteins. However, drug delivery systems usually burst and leak the payloads in the initial stage, and suffer from slow diffusion of the payloads in the treatment stage.[33–35,181,182] This phenomenon not only leads to drug loss during storage and blood circulation but also results in low intracellular drug availability. Efficient delivery has various requirements, such as stability during circulation, delivering payloads to specific sites, and releasing in a desired manner. Two main strategies are usually applied to meet such requirements: stimuli-induced aggregate structural variation and stimuli-induced mobility enhancement of the payloads.

Polypeptide aggregates are good candidates for delivery vehicles due to the following characteristics.[9–12] (1) Polypeptide-based copolymers can self-assemble into core–shell aggregates in aqueous solution. The aggregate morphology and structure can be tuned through the polymer composition, preparation conditions, polypeptide conformation, and introduction of secondary components. (2) Water-soluble ionic polypeptides such as PLGA and PLL can be used to bind drugs bearing opposite charge. When the solution pH changes, the binding ability of the polypeptide to the drugs decreases, inducing rapid drug release. (3) Polypeptides usually contain a large amount of reactive groups,

such as carboxylic groups and amino groups. These reactive groups can be applied to conjugate drugs with labile chemical bonds, which can be broken under certain conditions to release the payloads. In the following section, research concerning drug-release behaviour under physical or chemical stimuli is discussed.

3.1 Release behaviour regulated by the binding ability between polypeptides and payloads

For drug deliveries, payloads are incorporated into aggregates through physical or chemical means. In physical methods, payloads are physically encapsulated in the aggregate cores. To prevent leakage of the drug during storage and delivery, a strong physical attraction between polymers and payloads is essential. Hydrophilic ionic polypeptides, such as PLGA, PAsp, and PLL, can bind payloads through electrostatic attraction.[36–39] In chemical methods, payloads are covalently conjugated to core-forming or shell-forming polypeptide blocks *via* stimuli-responsive cleavable bonds. When the external surrounding conditions change, for example, a variation in the solution pH, the chemical bonds between the polymers and payloads can be broken, which induces the release of drugs from the aggregates.[40–42] In the following section, changing the binding ability of polypeptides to regulate the release of payloads through both physical and chemical strategies is reviewed.

3.1.1 Release of payloads regulated by decreasing electrostatic attraction. Among the various physical interactions, electrostatic attraction is especially important in controlling the release of payloads from polypeptide aggregates.[183–187] Electrostatic attraction can prevent the bursting and release in the initial stage, and the electrostatic attraction between the polymers and drugs can be easily weakened by adjusting the pH, which thus induces a rapid release of the payloads at the target sites. Smart drug carriers have been designed and constructed by making use of the electrostatic attraction between charged polypeptides and payloads, for example, PLGA *vs.* cationic DOX and PLL *vs.* anionic DNA.

Hong *et al.* developed drug-loaded micelles using anionic PEG-*b*-PLGA and the cationic anticancer drug doxorubicin (DOX) for cancer treatments.[186] DOX was loaded into the micelles *via* electrostatic interactions (between COO^- of PLGA and NH_3^+ of DOX) and hydrophobic stacking (among the DOX molecules). A high loading efficiency was achieved (Fig. 9a) and the DOX-loaded micelles exhibited a negative surface charge around −30 to −40 mV (Fig. 9b). As shown in Fig. 9c, the release rate of DOX from the micelles was slower at physiological pH, but it clearly increased in acidic pH environments. The increased release of the drug is related to the decreased binding ability of PLGA with DOX due to the protonation of the COO^- groups of the PLGA chains in acidic solution. Cellular uptake and cytotoxicity studies suggested that micelles are taken up by A549 cells *via* endocytosis, with a slightly slower cellular internalization and lower cytotoxicity compared with free DOX. The *in vivo* pharmacokinetic study demonstrated the significant advantages of DOX-loaded micelles (Fig. 9d), including prolonging the blood circulation time, enhancing the therapeutic efficacy,

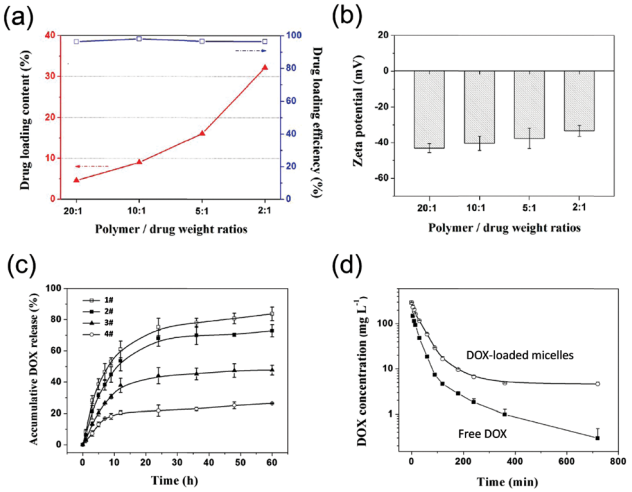

Fig. 9 (a) Drug loading content and drug loading efficiency at different weight ratios of polymer to DOX; (b) zeta-potential of DOX-loaded micelles at different weight ratios of polymer to DOX; (c) time and pH-dependent DOX release profiles of DOX-loaded micelles in PBS at pH 5.5 with 10% FBS (1#), PBS at pH 5.5 (2#), PBS at pH 7.4 with 10% FBS (3#), and PBS at pH 7.4 (4#); (d) *in vivo* pharmacokinetic profiles after intravenous injection of free DOX and DOX-loaded micelles in rats. Reprinted with permission from ref. 186. Copyright 2013 American Chemical Society.

increasing apoptosis in tumour tissues, and reducing systemic toxicity. These results demonstrate that the PEG-*b*-PLGA smart micelle is a promising vehicle to improve the pharmacokinetics and efficacy of drugs with reduced toxicity.

Zhang *et al.* used cationic PLL-based polypeptide micelles to deliver anionic DNA.[187] A series of PEG-*b*-PLL-*b*-PLP triblock copolymers were synthesized. These copolymers self-assemble into micelles with hydrophobic PLP (poly(L-phenylalanine)) chains as the core and hydrophilic PEG-*b*-PLL chains as the shell. Cytotoxicity studies revealed the good biocompatibility of the copolymers. The micelles exhibit pH sensitivity in their hydrodynamic size and drug release behaviour, which is attributed to the protonation/deprotonation of amino groups in the PLL chains at different pH values. By increasing the pH from 4 to 10, the hydrodynamic diameter of the micelles decreases from approximately 60 nm to 15 nm. This pH-induced size variation is related to the deionization of amino groups in the PLL chains at higher pH, which decreases the repulsion between the PLL chains and leads to a smaller hydrodynamic diameter. The micelles possess excellent controlled drug release properties and apparent disparities in drug release rates at different pH values. *In vitro* transfection demonstrated that DNA-loaded PEG-*b*-PLL-*b*-PLP triblock copolymer micelles have a high transfection efficiency in 293T cells with low cytotoxicity under optimized conditions.

The electrostatic attraction is a strong interaction, which ensures high efficiency in drug loading and minimizes drug leakage during delivery. However, in practice, the situation is usually rather complex. For example, in the presence of ionic biomolecules, such as serum and heparin at the targeting site in the body, the loaded drugs could readily depart from the polypeptide chains and rapidly release into the delivery site.

In addition, the release of drugs can decrease the stability of the drug-loaded micelles, which further accelerates the drug release rate. Therefore, in practice, the electrostatic attraction between drugs and polypeptides is effective in loading certain specific drugs; however, these drug-loaded micelles could be unstable during delivery, and a fast leakage of the drugs may occur. Anyway, such a strategy is effective in preparing polypeptide-based drug deliveries, and could meet the application demands in some occasions. It is still essential to design polypeptide copolymers with optimal chemical composition and topology to achieve balance among the loading capacity, delivering stability, and releasing behaviour.

3.1.2 Release of payloads regulated by breaking labile chemical bonds. The chemically conjugated drug-loaded micelles have advantages in controlling the release of drugs, which can protect drugs from the host defence system during the delivery and release of drugs into the target tissues triggered by specific stimuli.[188–190] Such a strategy improves both the delivering stability and the therapeutic efficiency of the drugs. The reactive side groups of polypeptides endow polypeptide copolymers with advantages in constructing chemically conjugated drug-loaded micelles.[40–42] Various stimuli-labile bonds including acid-labile hydrazone bonds and GSH-reducible disulphide bonds are applied in chemically conjugated, drug-loaded delivery systems constructed from polypeptide micelles.

Kataoka and co-workers reported a number of examples of drug-loaded micelles prepared by a chemical strategy.[191–193] Fig. 10a shows a model of the polypeptide copolymer/drug conjugates. They prepared a targeted and pH-sensitive micellar drug carrier from Fol-PEG-*b*-P(Asp-Hyd-ADR) (Fol: folate; Hyd: hydrazine; ADR: adriamycin) drug-conjugated polypeptide block copolymers (Fig. 10b).[191] Folate on the surface of the micelle targets cancer cells, and the anticancer drug ADR is connected to the side chain of the core-forming PAsp segment through an acid-sensitive hydrazone bond. As represented in Fig. 10c, the drug-loaded micelles can be guided to the cancer cells in the body. After the micelles enter the cells, in the intracellular acidic environment (pH 5–6), hydrazone bonds are cleaved and DOX is released.

Lin *et al.* applied both physical and chemical strategies to encapsulate two drugs in a single polypeptide micelle.[79] Two model drugs, DOX and naproxen (Nap), were loaded into PPO-*b*-PBLG-*b*-PEG triblock copolymer micelles (Fig. 11a). Spherical micelles with PEG corona, PBLG/DOX shells, and PPO/Nap cores were formed with diameters of approximately 150 nm, which means that these micelles are suitable drug-delivery vehicles. In the micelles, DOX is chemically linked to PBLG backbones through an acid-cleavable hydrazone bond, whereas Nap is physically encapsulated in the cores. This core–shell–corona structure was further elucidated by DPD simulations (Fig. 11b). *In vitro* studies revealed pH- and thermo-sensitive release of DOX and Nap from the micelles. As shown in Fig. 11c, due to the cleavage of the hydrazone bonds, the release rate of DOX is faster in acidic solutions. Furthermore, because PPO dehydrates at higher temperatures, a faster release of the two drugs can be observed at higher temperatures. By adjusting the

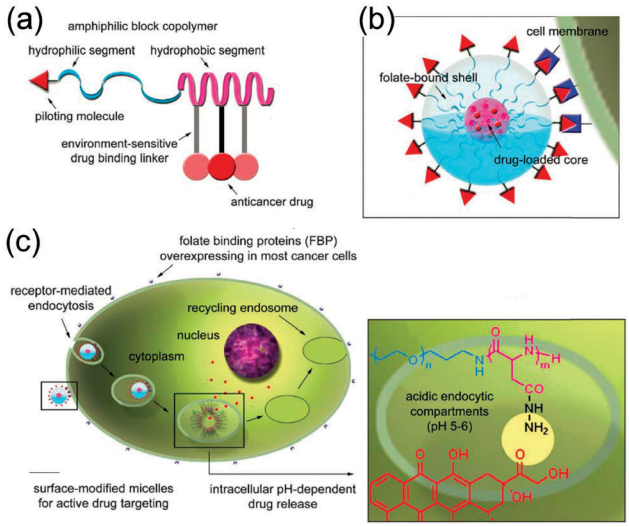

Fig. 10 (a) Model of a drug-conjugated polypeptide polymer. (b) Typical structure of self-assembled micelles. (c) Polymer micelles with tumour selectivity for active drug targeting and pH sensitivity for intracellular site-specific drug transport. Reproduced from ref. 191 with permission from The Royal Society of Chemistry.

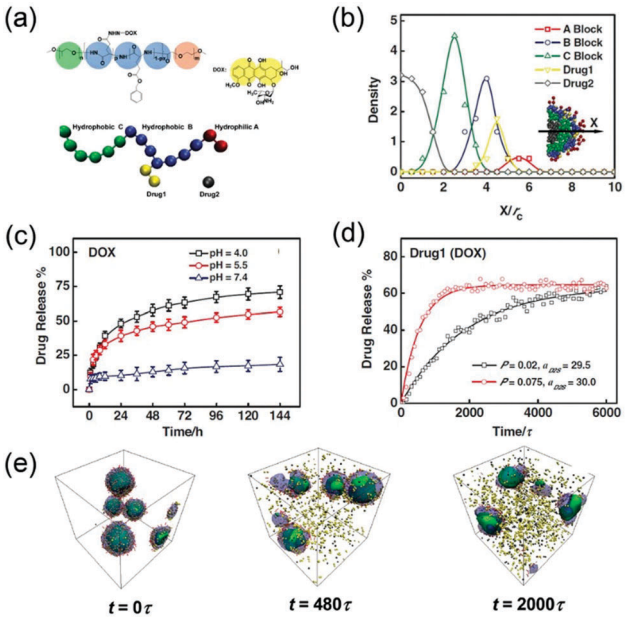

Fig. 11 (a) Mapping between the experimental sample and DPD simulation model. (b) Density profiles along the x-arrow of different segments of terpolymer/drug micelles. The red, blue, green, yellow, and black colours are respectively assigned to A, B, C, Drug1, and Drug2, and the solvents are omitted for clarity. (c) The influence of pH on the release profiles of DOX from dual-drug-loaded micelles. T = 37 °C. (d) Simulation of the release of Drug1 (DOX) from dual-drug loaded micelles under various pH conditions. The case of P = 0.02 and a_{D2S} = 29.5 corresponds to a higher pH condition, whereas the case of P = 0.075 and a_{D2S} = 30.0 corresponds to a lower pH condition. (e) Typical simulation snapshots of the release of Drug1 and Drug2 at P = 0.075 and a_{D2S} = 30.0. The simulation times are t = 0, 480, and 2000τ. Reprinted with permission from ref. 79. Copyright 2014 Wiley-VCH.

experimental conditions to align with the simulation parameter settings, they simulated the release behaviours of the drug carriers. The simulations reproduced the experimental observations well. Fig. 11d shows the simulation results for the release behaviour of DOX as a function of solution pH. In the figure, P and a_{D2S} represent the probability of breaking the bond between DOX (Drug1) and the PBLG blocks and the interaction parameter between Nap (Drug2) and water, respectively. The case of $P = 0.02$ and $a_{D2S} = 29.5$ corresponds to a higher pH condition, whereas the case of $P = 0.075$ and $a_{D2S} = 30.0$ corresponds to a lower pH condition. In addition to representing the release behaviours, the simulations suggest that the entire micellar structure remains unchanged during the release, but its size decreases gradually with time (Fig. 11e).

Lin *et al.* also carried out *in vitro* cytotoxicity and uptake studies. The results reveal that these dual-drug-loaded micelles significantly improve the biocompatibility and retention time of drugs and therefore enhance the therapeutic effects of the drugs. Furthermore, these biocompatible dual-drug-loaded micelles can enter cells and release drugs in the cytoplasm. These results demonstrate that polypeptide copolymer micelles can be utilized to deliver multiple drugs that act on the same cells, maximizing the therapeutic effect. The significant advantage of this work is the combination of experiments and simulations to study the structure and the release behaviour of drug-loaded micelles. For the polymer micelle drug delivery systems, a number of studies have been reported, but the release mechanisms are still not well understood due to the limitation of the currently available experimental techniques. Theoretical simulations conducted on the basis of experimental observations can address these challenges because they can provide straightforward microscopic information.[69–73,76–81] For example, Buxton and co-workers developed a new coarse-grained simulation method, which captures the dynamics of the polymer nanoparticle and the diffusion of the encapsulated drug.[194,195] Using this method, they simulated the drug release performance of nanoparticles with a pH-responsive shell material. An increased release rate of a chemotherapeutic agent near tumours was observed. The interactions between the DDS and the plasma membrane were also studied with the help of simulations. Zhang *et al.* performed DPD simulations of the pathways of vesicle/liposome–membrane interactions.[196,197] The pathways of interaction may be varied under different DDS or membrane conditions. The procedures of cellular internalization, even the transformation and drug release performance of the DDS were clearly shown. Those simulation works not only support experimental investigations, but also provide molecular-level insight into the drug delivery behaviours, which greatly benefits the design of desirable DDSs.

Compared with the physical loading method, conjugating drugs to a polypeptide backbone through chemical bonds can enhance the stability of carriers and decrease the toxicity of the drugs. The chemically conjugated drug-loaded micelles are efficient in loading drugs and controlling the release of drugs. However, the premature release of drugs during delivery still occurs with chemically conjugated drug-loaded micelles. For example, when the drug-loaded micelles are exposed to acidic intercellular surroundings, the labile chemical bonds between the polypeptide backbone and payloads can break, which consequently induces rapid release of the payloads before arrival at the target sites. To improve delivery performance, several strategies such as crosslinking the deliveries could be effective in reducing the premature release of drugs.

3.2 Release behaviour regulated by the structural variation of aggregates

Stimuli-induced structural variation of polymer aggregates, such as reassembly and disassembly, is extremely useful for the triggered release of payloads in targeted tissues and intracellular compartments.[198,199] Both physical and chemical processes, for example, conformation transition and deprival of the side groups of polypeptide chains, can induce reassembly and/or disassembly of aggregates.[43,44,200–208] Such features can be applied to design stimuli-sensitive drug deliveries from polypeptide-based copolymers. The aforementioned stimuli-sensitive behaviours are generated from polypeptide chains, and those induced by non-polypeptide chains are outside of the scope of this article.

3.2.1 Solubility and conformation changes of polypeptide chains. External stimuli, such as pH and temperature, may induce a conformation transition of polypeptide chains as the solubility of the polypeptide chains changes. With the variation of polypeptide conformation and solubility, the self-assembly structure of polypeptide aggregates can be varied.[200–204] In some cases, the aggregates even disassemble into single chains. As a result, the physically encapsulated drugs and other payloads can be quickly released from the aggregate.

Qiao *et al.* reported the pH-induced reassembly of polypeptide micelles self-assembled from PEG-*block*-poly(D,L-lactide)-*block*-poly(L-histidine) (PEG-*b*-PLA-*b*-PHis) to trigger the release of payloads.[203] The micelles consist of PLA and unprotonated PHis blocks as the hydrophobic core and PEG as the hydrophilic shell at neutral pH. Reassembly of the micelles in acidic environments was observed, which triggered the release of physically incorporated DOX. These DOX-loaded micelles are promising pH-sensitive delivery vehicles. For example, when the micelles enter endolysosomes (acidic environment) after endocytosis, the PHis block is protonated and the micelles reassemble, which subsequently induce the release of the incorporated drugs from the micelles.

In addition to the single copolymer systems, copolymer mixture systems have also been applied to construct "smart" drug delivery systems.[209–211] Polypeptide copolymer mixtures advantageously control the structure and function of the delivery. Lin *et al.* designed and constructed hierarchical micelles from a mixture of two block copolymers for drug delivery applications.[204] They first constructed a simulation model containing $A_{10}B_7A_{10}$ triblock copolymers and B_1C_3 diblock copolymers, and then used MD simulations to predict the self-assembly behaviour of the polymer mixtures and the structure of the hierarchical micelles. The simulation results revealed that micelles with B blocks as a core and A and C blocks as a mixed corona were formed (Fig. 12a). With a change in the solubility of the

corona-forming A blocks, a structural variation of the micelles was predicted, *i.e.*, formation of a channel in the micelle corona (Fig. 12b). The formation of a channel in the polymer micelle is interesting, and such a microstructure could be useful in designing and constructing "smart" drug delivery systems. Under the guidance of the simulation predictions, they prepared a polypeptide-based drug delivery system containing PLGA-*b*-PPO-*b*-PLGA and PEG-*b*-PPO block copolymers. DOX was used as a model drug. For the drug delivery vehicles, PPO blocks formed the core, and PLGA and PEG blocks formed the corona. Under basic conditions, the flexible PLGA and PEG chains are well mixed, forming the corona of the micelles, which is unfavourable for drug release. As the pH value decreases to acidic levels, the solubility of PLGA worsens. Therefore, the PLGA chains collapse and phase separate from the PEG chains, resulting in the formation of a PEG channel, as predicted by the simulations. Meanwhile, the collapse of the PLGA chains generates stress on the core of the micelles, inducing a faster release of the drugs from the hierarchical micelles through the PEG channels. This pH-sensitive structural variation accelerates the release of DOX (Fig. 12c). These hierarchical micelles exhibit a highly tunable drug release behaviour in response to a change in the external pH without sacrificing the colloidal stability. A proposed scheme representing the pH-sensitive release mechanism of the PLGA-*b*-PPO-*b*-PLGA/PEG-*b*-PPO drug-loaded micelles is presented in Fig. 12d. Theoretical simulation shows the important role in designing drug carriers. Under the guidance of simulation predictions, it is possible to construct polypeptide drug carriers with designed structures and functions. Because experimentally screening premium structures for drug carriers is a daunting task, designing with assistance of simulations is clearly useful and essential to build effective drug delivery systems. Conducting experiments under the guidance of simulation predictions can significantly improve the efficiency of the prepared efficient carriers.

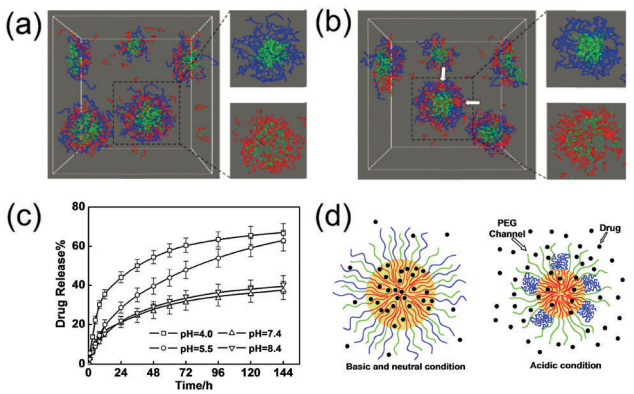

Fig. 12 (a and b) Typical simulation snapshots of $A_{10}B_7A_{10}$ triblock copolymer and B_1C_3 diblock copolymer self-assemblies: (a) both A and C blocks dissolve well in solution and (b) the solubility of the A block decreases. The blue, green, and red lines represent the A, B, and C blocks, respectively. Arrows point to the C block aggregation areas. (c) Experimental results for the release of DOX from hierarchical micelles formed by mixtures of PLGA-*b*-PPO-*b*-PLGA/PEG-*b*-PPO with a ratio of 5/5 (wt/wt) at various pH values. (d) Schematic representation of the pH-sensitive release mechanism proposed for the hierarchical micelles. Reprinted with permission from ref. 204. Copyright 2009 Elsevier B.V.

3.2.2 Cleavage of side groups from polypeptide chains. Reactive side groups on polypeptide chains, such as –COOH and $–NH_2$, are useful for conjugating hydrophobic moieties onto polypeptide copolymers. When the chemical bonds are cleavable under external stimuli, such as acid, light, and temperature, stimuli-responsive polypeptide aggregates can be constructed by assembling these polypeptide copolymers.[205–208] With the cleavage of the chemical bonds, the hydrophobic moieties leave the polypeptide chains, which shifts the hydrophilic–hydrophobic balance and induces a reassembly or disassembly of the aggregates. As a result, the physically incorporated payloads can be rapidly released from the polypeptide delivery system.

Kwon *et al.* prepared PEG-*block*-poly(ketalized serine) (PEG-*b*-poly(kSer)) micelles that served as a pH-sensitive DNA delivery system.[206] Upon acid-hydrolysis of ketal linkages, the amino ketal moieties depart from the polypeptides, and hydrophobic poly(kSer) converts to hydrophilic poly(serine). Therefore, the DNA-loaded micelles disassemble and release DNA. As shown in Fig. 13a, DLS testing revealed that the diameter of the PEG-*b*-poly(kSer)/DNA micelles markedly increases with hydrolysis at pH 5.0, which indicates that the micelle structure has been destroyed and loosened. The TEM images presented in Fig. 13b provide direct evidence for the increase in the diameter of the micelles. Such disassembly triggers the rapid release of loaded DNA under acid conditions. *In vitro* studies demonstrated that, due to their ability to disassemble, PEG-*b*-poly(kSer)/DNA micelles are more efficient than PEG-*b*-PLLys/DNA micelles and PLlys/DNA polyplexes in transfecting NIH 3T3 cells. Developing safe and efficient gene transfer methods is an indispensable technological requirement for achieving clinical success for gene therapy. This study demonstrates that acid-transforming micelles are promising carriers for stimuli-responsive and targeted drug/gene delivery.

Light-sensitive micelles are important candidates for drug delivery applications, which can trigger drug release at a designed time at a light exposure site by turning on/off a light.[212–214] Dong *et al.* used UV light to trigger the release of DOX from poly(*S*-(*o*-nitrobenzyl)-L-cysteine)-*b*-PEG (PNBC-*b*-PEG) polypeptide micelles by varying the structure of the PNBC-*b*-PEG micelles.[215] Under UV exposure, the UV-sensitive *o*-nitrobenzyl groups are cleaved from the hydrophobic PNBC chains, which induces the structural variation of the micelles. After UV irradiation, a decrease in aggregate size was observed, which was induced by cleaving the *o*-nitrobenzyl groups from the core-forming PNBC chains. As a result, the physically loaded DOX is released from the micelle. In addition, the release rate can be controlled by changing the duration of light irradiation.

Compared with UV or visible light, near-infrared (NIR) light is more suitable as a stimuli source in biomedical applications because it penetrates deeper into live tissues and is less harmful to healthy cells.[216–218] Zhao *et al.* reported the NIR light-triggered release of drugs from polypeptide micelles.[218] Polypeptide block copolymers composed of PEO and PLGA bearing a number of 6-bromo-7-hydroxycoumarin-4-ylmethyl

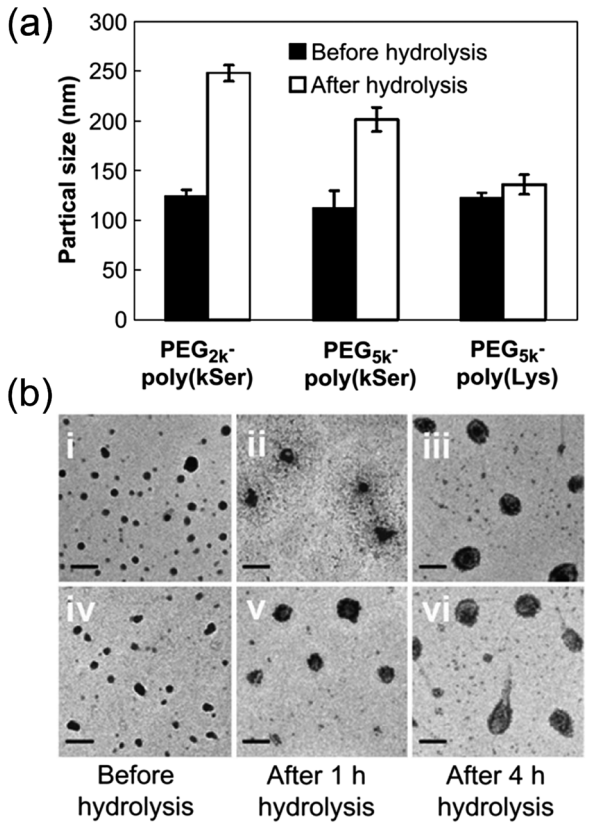

Fig. 13 (a) Particle diameters of various PEG-*b*-polypeptide/DNA micelles before and after hydrolysis at pH 5.0 for 4 h at 37 °C. (b) TEM images of PEG5k-*b*-poly(kSer)/DNA (i–iii) and PEG2k-*b*-poly(kSer)/DNA micelles (iv–vi) before and after hydrolysis in pH 5.0 buffer for 1 and 4 h. Scale bar: 200 nm. Reprinted with permission from ref. 206. Copyright 2010 Elsevier B.V.

groups (COU), PEO-*b*-P(LGA-*co*-COU), were synthesized. Under the excitation of 794 nm NIR light, the chemical bonds between the coumarin moiety and the polypeptide backbone could be broken, disrupting the micelles. The removal of coumarin groups from the polypeptide block shifts the hydrophilic–hydrophobic balance, which further destabilizes the micelles. This characteristic is useful for designing and preparing NIR light-triggered drug release carriers. By loading model drugs (Rifampicin and Paclitaxel) into the PEO-*b*-P(LGA-*co*-COU) micelles, Zhao *et al.* found that the drugs could be effectively released upon NIR light exposure of the micellar solution.

Variation of the chemical structure of polypeptide chains, such as removal of hydrophobic moieties, usually leads to a hydrophobic-to-hydrophilic transition of the polypeptide chains, which further decreases the stability of the aggregates. As a result, release of physically loaded payloads is achieved. Diverse bonds that are cleavable by specific stimuli, including acid, UV light, and NIR light, are applied in such systems. Among these stimuli, pH is commonly used to cleave the chemical bonds with high efficiency, which further triggers the removal of hydrophobic moieties from polypeptide chains. For example, the local pH value in some target tissues is significantly lower; therefore, pH-sensitive delivery systems that can remove hydrophobic moieties and release payloads under acidic conditions are favourable. In addition, light is an excellent tool to trigger drug release because it is safe and easily operated from outside of the body. However, one of the main obstacles is that light cannot reach inner tissues of the body. Therefore, suitable applications of light stimulus systems could be limited to treating diseases of the skin, in which light can have a great effect. Selecting an appropriate stimulus based on clinical demands can not only provide high efficiency in drug delivery but also simplify clinical treatment. More work is needed to design and prepare carriers that meet various clinical demands.

3.2.3 Dis-crosslinking of crosslinked aggregates. Covalent crosslinking the core or shell of the drug delivery carrier has emerged as a viable strategy to significantly improve the stability of delivery vehicles and reduce the premature release of payloads during transport.[219–222] However, crosslinked micelles usually present difficulties in drug release because of their increased stability. Therefore, it is essential to break the crosslink bonds under an external stimulus.[223–225] Remarkable progress has been made in developing stimuli-responsive crosslinked micelles, including pH-cleavable, disulphide-bond-containing, and hydrolysable ester-bond-containing crosslinked micelles. Polypeptides and their deliveries are chemically functionalizable with various reactive groups that can be applied to crosslink the polypeptide chains. When the crosslinked bonds are broken by a stimulus, including lower pH, higher temperature, or a higher concentration of glutathione (GSH) or other expressed enzymes, disassembly of the polypeptide-based crosslinked micelles usually occurs in the target tissues.[226–228] Making use of such characteristics, it is possible to construct efficient polypeptide-based drug delivery systems that are stable during circulation and can release payloads at specific sites in a desired manner. The following section features research on the release of drugs induced by dis-crosslinking of polypeptide micelles.

Zhong *et al.* developed reversibly core-crosslinked (CCL) polypeptide micelles with dual sensitivity to reduction and pH from PEG-*b*-P(LL-CCA/LA) block copolymers decorated with lipoic acid (LA) and *cis*-1,2-cyclohexanedicarboxylic acid (CCA).[229] The crosslinked micelles exhibit high stability against extensive dilution (Fig. 14a). As shown in Fig. 14b, *in vitro* studies reveal that the release of physically loaded DOX at pH 7.4 is significantly inhibited by crosslinking. However, under reducing conditions containing glutathione (GSH), rapid DOX release was observed, which resulted from the dissociation of the micelles into unimers. The cellular uptake (HeLa cells) and intracellular drug release behaviours of DOX-loaded crosslinked micelles were further investigated using CLSM. As shown in Fig. 14c, DOX is delivered and released into the nuclei of cells following a prolonged incubation time of 12 h. The observations of intracellular drug release are in line with the high anti-tumour activity of DOX-loaded crosslinked micelles, confirming that pH- and reduction-sensitive crosslinked micelles promote fast intracellular drug release. These responsive core-crosslinked polypeptide micelles appeared to be an advanced platform for cancer therapy.

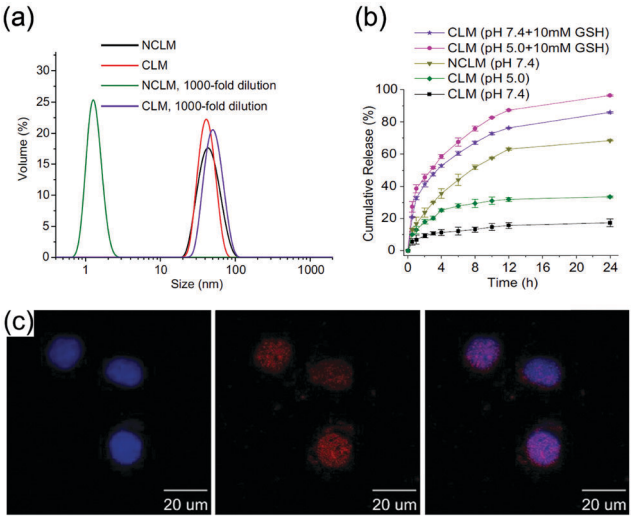

Fig. 14 (a and b) Properties of the core-crosslinked PEG-*b*-P(LL-CCA/LA) micelles: (a) colloidal stability of the micelles against 1000-fold dilution, (b) *in vitro* release of DOX at pH 7.4 or 5.0 in the presence or absence of 10 mM GSH. (c) CLSM images of HeLa cells incubated with DOX-loaded crosslinked PEG-*b*-P(LL-CCA/LA) micelles for 12 h. The images from left to right show cell nuclei stained by DAPI (blue), DOX fluorescence in cells (red), and overlays of the two images. Reprinted with permission from ref. 229. Copyright 2013 Elsevier B.V.

In addition to CCL polypeptide micelles, shell crosslinked (SCL) polypeptide micelles are also employed as delivery vehicles. Zhang *et al.* prepared SCL drug carriers from PEG-*b*-poly(L-cysteine)-*b*-poly(L-phenylalanine) (PEG-*b*-PCys-*b*-PPhe) triblock copolymers.[230] The copolymers self-assemble into core–shell–corona micelles in aqueous solutions. The shells of the micelles can be crosslinked by oxidation of the thiol groups in the PCys segments. As indicated by DLS testing, by increasing the volume percentage of DMF in the micelle solution, the SCL micelles could maintain their micellar structure with an increase in diameter, whereas non-crosslinked micelles dissociated, resulting in a sharp decrease in the observed scattering intensity. *In vitro* drug release studies revealed that crosslinking of the shell significantly reduces drug loss in the extracellular environment. In the presence of GSH, the crosslinked disulphide bonds are cleaved, which accelerates drug release from the micelles. These GSH-responsive SCL micelles show potential for use in intracellular drug delivery. For example, these SCL micelles were successfully internalized by HeLa cells after 4 h of incubation, with demonstrated enhanced cytotoxicity.

Ideal drug delivery systems are required to be stable in circulation, while instable at targeted sites to induce rapid drug release. *In vitro* studies revealed that crosslinking the core/shell of micelles can effectively restrain premature drug release and improve drug accumulation. With the cleavage of crosslinking bonds in the intracellular environment, accelerated drug release from the micelles can be achieved in the target tissues. Further achievement should be done to meet the practical clinical demands. For example, according to the release rate of the drugs in specific targets, the cleavage rate of crosslinking bonds should be controllable. In some cases, breakage of the crosslinked vehicles to give a burst release of payloads is necessary. Under such conditions, a complete degradation rather than discrosslinking should be necessary. Furthermore, the *in vivo* microenvironment is complex, which could disrepute a precise spatiotemporal drug release. With the guidance of practical clinical demands and the feedback, high efficient delivery vehicles with delicate structure and function should be designed.

3.3 Release behaviour regulated by the chirality of polypeptides

Compared with normal polymers, polypeptides are chiral polymers built from L- or D-form units.[30–32] When L- and D-form peptide units are copolymerized, achiral polypeptides (poly(racemic-amino acid)) can be obtained. The chirality of polypeptides imparts many unique characteristics to polypeptide copolymers. For example, poly(levo-amino acid) or poly(dextro-amino acid) has a rigid α-helix conformation, whereas poly(racemic-amino acid) is a flexible polymer. However, the effect of polypeptide chirality on the properties of the carrier such as drug loading, delivery, and release has not been well documented to date. Few existing studies have demonstrated that changing the chirality of the polypeptide can influence the properties of polypeptide DDSs.[231–236]

Gu *et al.* synthesized racemic polypeptide copolymers with different leucine residues (PEG-*b*-poly(racemic-leucine) (PEG-*b*-PRL)).[235] As revealed by the CD spectra in Fig. 15a, the PRL segments appear as flexible chains while PLL segments are in rigid α-helix conformation. The assemblies of these PEG-*b*-PRL racemic block polypeptides were applied as drug carriers using hydrophobic docetaxel (DTX) as a model drug. As shown in Fig. 15b, spherical particles with tunable sizes from 170 to 250 nm were obtained by changing the length of the hydrophobic blocks. Compared with the corresponding L forms (PEG-*b*-PLL), a higher drug-loading ability and an easier drug-loading process of the racemic hybrid polypeptide-based copolymer

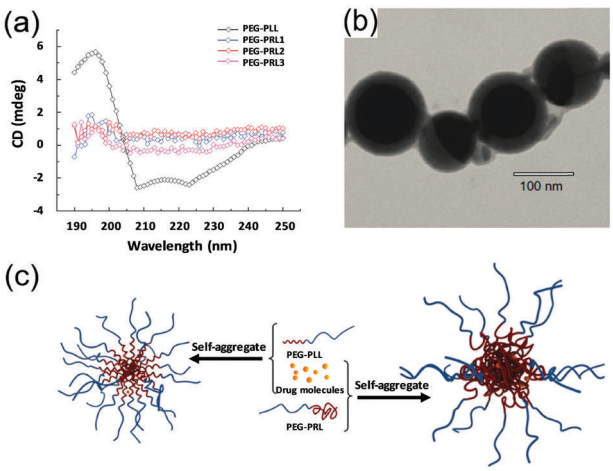

Fig. 15 (a) CD spectra of various PEG-*b*-polyleucine copolymers in aqueous solution. (b) TEM image of docetaxel-loaded PEG-*b*-PRL micelles. (c) Schematic representation showing the drug-loading process and self-assembly structure of micelles based on PEG-*b*-PLL and PEG-*b*-PRL copolymers. Reprinted with permission from ref. 235. Copyright 2012 Dove Medical Press.

assemblies were observed. The difference in drug loading between the two polypeptides hints that the chirality of the hydrophobic peptide block may play an important role in the drug-loading process. Such chirality-facilitated drug-loading behaviour is clearly interesting. They explained the main reason for the different drug-loading abilities of the PEG-*b*-PLL and PEG-*b*-PRL micelles as follows. As presented in Fig. 15c, the PLL blocks from PEG-*b*-PLL adopting an α-helical conformation are packed to form a rigid and compact hydrophobic micelle core, leaving a limited and restricted space for loading drug molecules. However, in the case of PEG-*b*-PRL, the PRL blocks are in a coiled conformation and form a relatively malleable and loose hydrophobic core, which could encapsulate many more drug molecules compared with PEG-*b*-PLL. These results indicate that racemic polypeptides could facilitate drug loading by providing a much higher drug-loading capacity compared with the corresponding levo or dextro forms.

Very recently, Ding *et al.* reported chirality-mediated polypeptide micelles from PLL-*b*-PEG-*b*-PLL and PRL-*b*-PEG-*b*-PRL triblock copolymers for regulated drug delivery.[236] In aqueous solution, the PLL-*b*-PEG-*b*-PLL and PRL-*b*-PEG-*b*-PRL amphiphilic copolymers self-assembled into spherical micelles with diameters of approximately 200 nm. The micelles with a racemic polypeptide core exhibited a smaller critical micelle concentration and diameter compared with those with a levo polypeptide core. Similar to that observed in Gu's work,[235] the PRL-*b*-PEG-*b*-PRL micelles exhibited higher drug-loading efficacy of DOX than those with a PLL core. This significant difference in drug-loading efficacy could be attributed to the flexible and compact PRL core of the micelle. Note that PLL takes a rigid α-helix conformation, whereas PRL takes a random coil conformation. Moreover, as revealed by *in vitro* release behaviour, the DOX-loaded PRL-*b*-PEG-*b*-PRL micelles are more durable during *in vitro* DOX release compared with the PLL-*b*-PEG-*b*-PLL micelles, which further contributes to the enhanced tumour inhibition efficacies and *in vivo* lower cytotoxicity of the former. These micelles appear to show great potential in smart antitumor drug delivery to lesion regions with enhanced chemotherapy efficacies and reduced side effects.

The chirality of the polypeptide chains is an important factor influencing the properties of drug carriers self-assembled from polypeptide copolymers. Compared with conventional copolymers, variation of the chirality of polypeptides gives the polypeptide micelle carrier special properties for drug delivery applications. Systematic and comprehensive investigations are still needed to identify the role of polypeptide chirality in nanostructure formation and explore the potential applications of these nanostructures as useful drug-delivery vehicles.

4. Polypeptide assemblies serve as biomimetic mineralization additives

Biominerals, acting as essential parts in living organisms, are well known for their hierarchical organization, complex shapes, controlled polymorphism, and superior properties.[45–47] Because of their fascinating characteristics, biominerals have intrigued scientists for decades due to the theoretical and practical values. Inspired by natural protein-controlled mineralization in organisms, biomimetic mineralization of inorganics in the presence of synthetic polymers is an attractive research topic.[48,49] Hydrophilic polypeptides such as PLGA, PAsp, PLL, and their derivatives have been used to mediate the mineralization of inorganics.[50–56] For example, Gower *et al.* found that PAsp homopolymers can induce a polymer-induced liquid-precursor (PILP) process in calcium carbonate ($CaCO_3$) crystallization to produce a helix superstructure.[50] Yu *et al.* used PEG-*b*-PLGA block copolymers to direct $CaCO_3$ crystallization and generate monodispersed vaterite microspheres.[51] Yamamoto *et al.* prepared helical $CaCO_3$ superstructures in the presence of PEG-*b*-PAsp block copolymers.[52]

However, hydrophilic polypeptides and their derivatives are structurally different from mineral proteins. Mineral proteins contain both hydrophobic and hydrophilic peptide units and fold into defined nanostructures. The amphiphilicity and folded structure of proteins play crucial roles in generating minerals with complex nanostructures. Amphiphilic copolymers containing hydrophilic polypeptide segments and hydrophobic polymers can self-assemble into diverse aggregates with defined structures, where the polypeptide segments resemble the charged peptide residues of minerals and the assembled structure can, to some extent, mimic the three-dimensional supramolecular structures of mineral proteins.[237–241] For example, Valiyaveettil *et al.* used self-assemblies of amphiphilic polypeptides as mimics of eggshell matrix proteins to tune the morphology of calcite since the self-assembling characteristics of polypeptides resemble the self-aggregation structure of proteins.[237] Therefore, polypeptide aggregates could be suitable candidates for the mediation of mineralization. Although there are only a few related examples, polypeptide aggregates are effective modifiers of crystal growth.

In this section, we focus on the biomimetic mineralization of inorganics in the presence of polypeptide self-assemblies. These polypeptide copolymers are classified into two types: those with both the hydrophobic and hydrophilic components derived from amino acids and those with polypeptide–nonpolypeptide copolymers containing hydrophilic polypeptide blocks and hydrophobic non-polypeptide blocks.

4.1 Mineralization mediated by polypeptide–polypeptide copolymer aggregates

From the aspect of chemical structure, full polypeptide-based copolymers that contain both hydrophilic and hydrophobic polypeptide segments exhibit similarity to natural mineral proteins.[59,60] These full polypeptide-based amphiphilic copolymers are capable of self-assembling into micelle-like aggregates in aqueous solution which can somewhat mimic the folded structure of natural proteins. Therefore, the full polypeptide-based copolymers can be applied as models for natural mineral proteins to study the protein-mediated mineralization of inorganics.

Meldrum *et al.* investigated the effect of aggregates self-assembled from aspartic acid and serine random copolypeptides

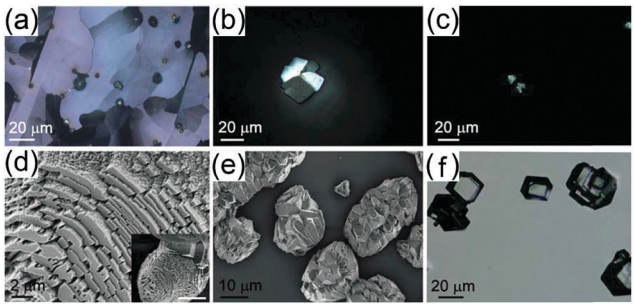

Fig. 16 Bulk crystallization of calcium carbonate in the presence of various random copoly(amino acid)s. (a–c) POM images of films formed at the air–water interface in the presence of (a) polypeptides containing 80 mol% aspartic acid residues (image recorded after annealing at 300 °C for 2 h), (b) polypeptides containing 50 mol% aspartic acid residues, and (c) polypeptides containing 20 mol% aspartic acid residues. SEM images of crystals formed in bulk in the presence of polypeptides containing 80 mol% aspartic acid residues and polypeptides containing 50 mol% aspartic acid residues are shown in (d) and (e), respectively. The inset in (d) gives an overview of the overall morphology of the crystal (scale bar: 10 mm). (f) Light microscopy image of rhombohedral calcite crystals grown in the presence of polypeptides containing 20 mol% aspartic acid residues. Reproduced from ref. 59 with permission from The Royal Society of Chemistry.

on the mineralization of $CaCO_3$.[59] A series of random copolypeptides constructed from aspartic acid and serine residues with various compositions were synthesized. The polypeptide random copolymers formed aggregates in solution with diameters ranging from 20 to 70 nm depending on the copolymer compositions. In the experiments, only the polypeptides containing 80 mol% aspartic acid residues induced the formation of continuous $CaCO_3$ films and roughened elongated particles at the air–water interface and in bulk solution, respectively (Fig. 16a and d). With polypeptides containing 50 mol% aspartic acid residues, relatively large, sheet-like patches precipitated but did not fuse into a continuous film at the water–air interface (Fig. 16b), and round particles formed in the solution that were coarser and more facetted than those observed with the polypeptide containing 80 mol% aspartic acid residues (Fig. 16e). However, polypeptides containing 20 mol% aspartic acid residues only mediated the formation of extremely small patches at the interface (Fig. 16c), and the bulk crystals took on a form of rhombohedra with smooth surfaces (Fig. 16f). These results therefore offer new insight into the relationship between polypeptide composition and mineralization behaviours and provide the basis for discussion of a highly acidic, protein-induced, biomineralization pathway from amorphous precursors.

The designed self-assembling structures of the polypeptide aggregates were able to promote the synthesis of crystals with a desired morphology. Stucky *et al.* investigated the crystallization behaviour of $CaCO_3$ under the mediation of aggregates formed by anionic, amphiphilic block copolypeptides, including poly(L-aspartate sodium salt)$_{100}$-*block*-(poly(L-phenylalanine)$_{25}$-random-(L-leucine)$_{25}$) (polymer 1) and poly(L-glutamate sodium salt)$_{100}$-*block*-(poly(L-phenylalanine)$_{25}$-random-(L-leucine)$_{25}$) (polymer 2).[60] The two copolymers self-assembled into aggregates approximately 65 and 55 nm in diameter, respectively. The self-assembled aggregates were able to act as templates to mediate the formation of $CaCO_3$ microspheres. The $CaCO_3$ microspheres were found to be composed of nanocrystals with sizes of 10 to 60 nm (polymer 1) or 20 to 100 nm (polymer 2). As a control experiment, they used random copolymers with similar chemical compositions to control the crystallization of $CaCO_3$. Because these random copolymers cannot self-assemble into defined aggregates, the resulting $CaCO_3$ morphologies are similar to those formed upon addition of poly(L-aspartate sodium salt) or poly(L-glutamate sodium salt) polypeptide homopolymers. This research emphasizes the importance of the aggregated structure of polypeptides in mediating the mineralization behaviour of $CaCO_3$ crystals.

4.2 Mineralization mediated by polypeptide–nonpolypeptide copolymer aggregates

As stated above, different from hydrophilic polypeptide additives, the amphiphilic polypeptide-based copolymers and natural proteins play two roles in the mineralization of inorganics.[242–244] First, the amphiphilicity of the copolymers enables them to self-assemble into diverse aggregates, which provide a suitable template for the nucleation of biominerals. Second, the hydrophilic part (usually ionic polypeptides) of the copolymers is able to bind with ionic species and further mediate the mineralization of inorganics. Therefore, the hydrophilic polypeptides are essential to mediate mineralization, whereas the hydrophobic polypeptides in the micelle core should have less effect on mineralization. Furthermore, synthesis of polypeptide–polypeptide copolymers is a daunting task. To simplify the synthesis process, aggregates formed by polypeptide–nonpolypeptide copolymers are applied as crystallization modifiers.[61–64] The polypeptide–nonpolypeptide copolymer aggregates also show high efficiency in mediating mineralization of inorganics.

Lin *et al.* used PLGA-*b*-PNIPAM block copolymers to mediate the mineralization of $CaCO_3$.[61] The effects of polymer unimers and aggregates on the biomimetic mineralization behaviour were compared. PLGA-*b*-PNIPAM block copolymers were synthesized by a combination of ROP and ATRP reactions. The PNIPAM is a thermo-sensitive polymer that possesses an LCST of approximately 33 °C. These block copolymers dissolve well in aqueous solution at 25 °C and self-assemble into micelles at 50 °C. On one hand, in the presence of PLGA-*b*-PNIPAM unimers at 25 °C, rosette-like $CaCO_3$ calcite crystals consisting of rhombohedral subunits are generated (Fig. 17a). The formation of such rosette-like crystals arises from a mesoscale self-assembly process in which the building units are temporarily stabilized by the copolymers and stacked irregularly due to the repulsive interactions among the polymer chains. On the other hand, the micelles formed above the LCST have a distinct effect on $CaCO_3$ crystallization. Fig. 17b and c present SEM and TEM images of $CaCO_3$ precipitates obtained in the presence of a 2.0 g L^{-1} micelle solution at 50 °C. The formed structures have a hierarchical coral-like cluster appearance, which is composed of aragonite fibres with lengths up to tens of micrometres (Fig. 17b). The fibres are covered with densely aligned nanorods parallel to one other (Fig. 17c). The nanorods are organized to

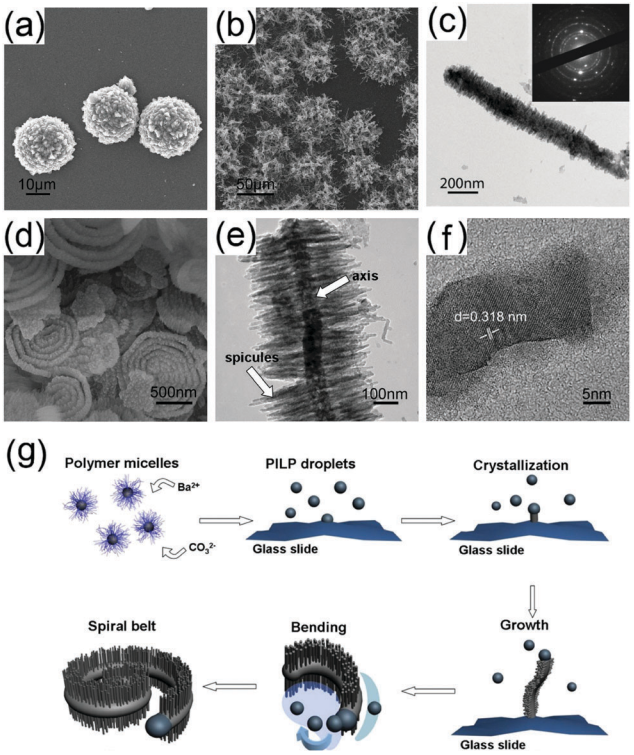

Fig. 17 (a–f) TEM and SEM images of the formed $CaCO_3$ and $BaCO_3$ crystals in the presence of PNIPAM-*b*-PLGA: (a) $CaCO_3$, 25 °C, SEM; (b) $CaCO_3$, 50 °C, SEM; (c) $CaCO_3$, 50 °C, TEM, the inset shows the SAED pattern of the fibre; (d) $BaCO_3$, 50 °C, SEM; (e) $BaCO_3$, 50 °C, TEM image of part of a formed spiral belt (the arrow on the left side points to the spicules, and the arrow on the right side points to the axis); and (f) $BaCO_3$, 50 °C, TEM image of a single spicule. (g) Proposed mechanism for the formation of a spiral. (a–c) Reproduced from ref. 61 with permission from The Royal Society of Chemistry. (d–g) Reproduced from ref. 14 with permission from The Royal Society of Chemistry.

some degree with polycrystalline structure indicated by the SAED pattern displaying obvious rings as shown in the inset of Fig. 17c. This research reveals that the polypeptide-based micelles and unimers play different roles in the crystallization of $CaCO_3$, which demonstrates the significant influence of the self-assembled structures of polymers on biomimetic mineralization.

Lin *et al.* also carried out studies on the mineralization of barium carbonate ($BaCO_3$) under the mediation of PLGA-*b*-PNIPAM micelles.[14] Interesting spirals were observed. Fig. 17d shows a typical SEM image of spiral structures. The spirals are constructed from crystal belts and can have up to eight circles. The nanostructure and growth orientation of the crystals were further characterized by TEM. Fig. 17e shows the TEM image of an individual crystal belt. The belt possesses a fishbone-like structure with spicules arranged in parallel along the thick axis. The spicules grow preferentially along *a*-axis, as judged by the lattice fringe distance of approximately 0.318 nm (Fig. 17f). These fibers could be formed through a solution–precursor–solid (SPS) process associated with the polymer induced liquid–precursor (PILP) mechanism under diffusion-limited conditions. The PILP phase is a highly hydrated, amorphous mineral precursor. In the SPS process, a growth point which possesses higher surface energies is created from the PILP droplets. The higher surface energies induce the preferential adsorption of PILP droplets on the growth point, resulting in one-dimensional growth of the crystals.[64,245,246] As shown in Fig. 17g, the liquid precursor of $BaCO_3$ is stabilized by PLGA-*b*-PNIPAM aggregates, which then serves as growth points for nanobelt growth. During crystallization of the PILP phase, the polypeptide aggregates are excluded, and the excluded polymers produce a concentration gradient of liquid droplets around the formed crystals. Therefore, the concentration gradient, which drives the growth direction, always tilts towards the direction of the formed nanobelt, resulting in the formation of a spiral structure. The spiral pattern of $BaCO_3$ produced in this research has similarity to that of some minerals discovered in nature, for example, the spiral pattern of aragonite on the inner surface of nacre. Such findings may provide a new strategy for the design of biomimetic minerals by applying polypeptide-based aggregates in mineralization.

The minerals mediated by polypeptide aggregates can be extended to bio-related applications, for example, drug delivery vehicles. Lee *et al.* reported the preparation of calcium phosphate (CaP) nanocarriers by polypeptide micelle-mediated mineralization for drug delivery (Fig. 18).[247] Drug-loaded micelles of PEG-*b*-PAsp-*b*-poly(L-phenylalanine) (PEG-*b*-PAsp-*b*-PPhe) were prepared as nanotemplates for mineralization. The micelles contain three distinct domains: the hydrophobic PPhe core, the anionic PAsp shell, and the solvated PEG corona. Inorganic CaP is selectively mineralized in the middle shells, acting as a diffusion-controlling barrier to drug release (Fig. 18a). The intracellular localization and drug-release properties of hybrid nanocarriers with mineralized shells were examined using confocal laser scanning microscopy (CLSM). As shown in Fig. 18b, after incubation for 30 min, almost all the DOX molecules have accumulated in the nucleus, and no molecules remain in the endosomes. It is clear that the DOX-PEG-*b*-PAsp-*b*-PPhe micelle-CaP is taken up by the cells *via* endocytosis. The material is transferred into endosomes and then into lysosomes to facilitate the release of DOX in the nucleus. In addition, the speed of drug release can be controlled by the thickness of the CaP shells.

Biomineralization is a complex process involving behaviour on many scales ranging from the atomistic scale to the mesoscale. Understanding this process can resort to theoretical simulations. It is better, yet difficult, to study the full process due to extremely large scales for simulations (from nanometers to microns, and from picoseconds to seconds). Most recent simulations were carried out at the atomic level, which can be helpful for understanding the peptide- or polypeptide-mediated crystallization process. Almora-Barrios and Leeuw applied MD simulations to investigate the early processes of the nucleation of hydroxyapatite in a collagen template.[74] A triple helical collagen molecule, which can be considered as a complex kind of polypeptides, is immersed in a stoichiometric solution of Ca^{2+}, PO_4^{3-}, and OH^- ions. The calculations of the interactions between a collagen peptide and the (0001) and (01$\bar{1}$0) surfaces of hydroxyapatite at body temperature (310 K) show a clear energetic preference for the peptides to absorb on the (01$\bar{1}$0)

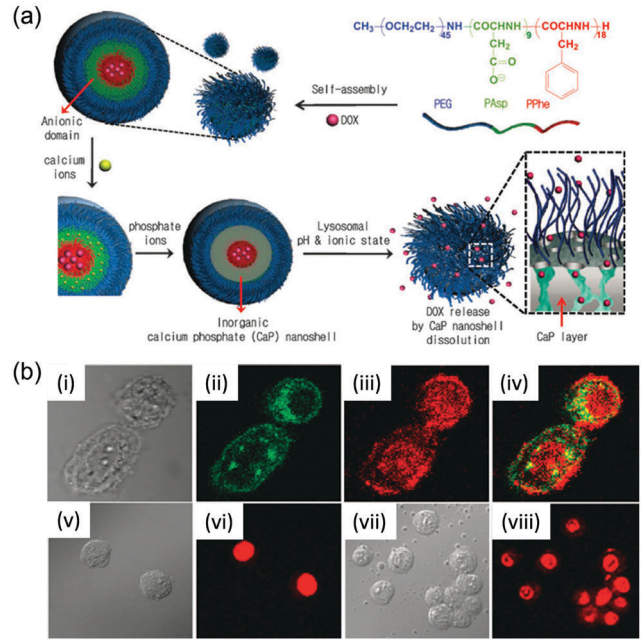

Fig. 18 (a) Illustration of the spatial mineralization of drug-loaded polymer micelles and facilitated drug release under specific intracellular conditions. (b) CLSM of MCF-7 cells (with GFP-labelled endosomes, green fluorescence) treated with DOX-PEG-*b*-PAsp-*b*-PPhe micelle-CaP for 30 min. (i) Differential interference contrast microscopy (DICM) image, (ii) green fluorescence (GFP), (iii) red fluorescence (DOX), (iv) overlap image of green and red fluorescence. DICM and CLSM images of cells treated with free DOX for 30 min (v and vi) and DOX-PEG-*b*-PAsp-*b*-PPhe micelle-CaP for 30 min (vii and viii). Reproduced from ref. 247 with permission from The Royal Society of Chemistry.

surface. Nucleation processes are affected by the interaction of the mineral phases with collagen peptides, which inhibits crystal nucleation and leads to morphologies closer to the natural materials. This can help to explain the biological morphology of the hydroxyapatite mineral where the $(01\bar{1}0)$ surface is expressed preferentially as a result of the growth-directing effect of the protein matrix. To understand whether a nucleation template for orientated hydroxyapatite could be formed in different peptide conformations, Sahai *et al.* conducted MD simulations to study the conformational effect on the distributions of Ca^{2+} and inorganic phosphate ions in solutions.[75] No apparent nucleation template for the hydroxyapatite crystal lattice is formed with different peptide conformations. They suggested that the templating effect with the α-helical conformation is not likely to be the dominant mechanism. Peter *et al.* performed the MD simulations to study the effect of the peptide sequence of several amphiphilic peptides on aggregate stability and ion–peptide interactions.[248] The results provided a valuable microscopic insight into the way that the ions and peptide templates mutually affect each other during the early stage of biomineralization preceding nucleation. In the presence of cations, peptide aggregates with Asp (aspartic acid) side chains were found to be less structurally stable than peptide aggregates with Glu (glutamic acid) side chains. This effect is relevant to templating mineral nucleation and growth in two possible ways. They suggested that the higher flexibility of the peptide aggregates with Asp side chains could be advantageous to support the growing mineral and the peptides with Glu side chains seem to be more suitable if template rigidity is relevant to the mineralization process. In addition to MD simulations, Muthukumar *et al.* presented a new model based on a competition between adsorption of polymers onto selective interfaces and nucleation growth of minerals.[249] The theory predicted the relative growth rates of different sectors altered by selective adsorption of polymers. The theoretical prediction of the dependence of the aspect ratio on polypeptide concentration was found to agree with experimental results. The main problem with the theory is that they require one to start with the knowledge of the structures that could emerge.

To our best knowledge, less attention has been paid to the mesoscale modeling of biominerals, which can help address the problems beyond classical crystallization theory. For example, the mesoscale simulations can provide useful information on biomineralization controlled by peptide aggregates. Camp and Lenoci used BD simulations to study the self-assembly of peptide and the formation process of biosilica spheres mediated by different peptide aggregates.[250] It was found that the model peptides self-assemble into spherical clusters, networks of strands, and bicontinuous structures, upon increasing the concentration of peptides. They suggested that the aggregates act as either nucleation points or scaffolds for the deposition of silica–peptide building blocks and there are two different scenarios each relevant to a different range of peptide concentrations. At low peptide concentrations small aggregates could provide nucleation surfaces from which amorphous silica spheres could expand radially, while at higher concentrations growing amorphous silica blocks would be confined by the surrounding peptide networks.

Despite the above examples, the simulation studies regarding biomineralization are limited. Simulation on the full process of biomineralization from atomistic scale to mesoscale crystallization could be the future directions in this field. Concerning the methods, attempts should be made to develop simulation techniques adaptable in a wide range of space scales and time-scales. It is also necessary to find a robust set of interactions that can connect different types of force fields in a physically sensible fashion for the simulations at different scales. Moreover, the simulation studies on polypeptide- or protein-mediated biomineralization are limited. There still remain a daunting variety of problems to be tackled such as the influence of the structure of polypeptide aggregates or proteins on the full process of mineralization.

Fundamentally, further investigation of polypeptide aggregate-mediated mineralization will deepen our understanding of the natural phenomenon of protein-mediated mineralization. In organisms, proteins mainly play two roles in biomineralization: (1) the polar peptide units concentrate ionic species, and (2) the hydrophobic peptide units serve as localized nucleation centres for crystallization. Polypeptide-based aggregates can play these two roles in mineralization. The soluble polypeptide blocks sequester ions, and the insoluble blocks (polypeptide or

non-polypeptide) act as nucleation centres. Therefore, polypeptide copolymer aggregate-directed mineralization could be considered as a model for studying protein-mediated biomineralization. In addition, because the composition and structure of polypeptide-based aggregates are highly modifiable, the specific effect of each block and the defined structure of the aggregates can be evaluated. The results obtained can be useful for explaining the biomineralization behaviour directed by natural proteins *in vivo*.

In applied science, it is expected that the polypeptide-based aggregates could be used to synthesize inorganic materials with hierarchical structures, because the synergistic effect between aggregated structures and polypeptide blocks can achieve precise control over the nucleation and assembly of nanoscale mineral building blocks.[244] In addition, it has been revealed that the copolymer aggregates can effectively incorporate within the lattice of crystals to form organic–inorganic composite materials.[251] Therefore, the polypeptide-based copolymer aggregates show great potential in the fabrication of organic/inorganic hybrid materials with specific macro- and microshapes and biocompatibilities that can be applied in drug delivery and tissue engineering. Many novel composite materials with useful properties are expected to be produced through this method in the future.

5. Concluding remarks and outlook

In this review, we presented a summary of recent advances in the construction of polypeptide-based copolymer self-assemblies for bio-related applications. The properties of polypeptides depend on not only the chemical structure but also the conformation structure. Due to the following characteristics, polypeptide-based copolymer self-assemblies are an attractive class of materials suitable for bioapplications such as delivery vehicles and biomimetic mineralization additives: (1) good biocompatibility derived from peptide components, (2) designable and well-defined nanostructures with various morphologies, (3) responsiveness to external stimuli through variation of the conformation and chemical structure of polypeptides, (4) small size and core–shell structure of assembled aggregates acting as delivery vehicles, and (5) assemblies that can mimic natural mineral proteins to act as biomimetic mineralization modifiers.

Benefitting from the development in polymer chemistry, copolymers with various architectures have been successfully synthesized. The architecture of amphiphilic copolymers is a fundamental factor determining the self-assembly structures. Many self-assembled structures have been observed from polypeptide-based copolymers. For example, polypeptide copolymers with $A(BC)_n$ molecular structure display unique self-assembly behaviours, as demonstrated in experiments and theoretical simulations. The self-assembly of polypeptide copolymers with complex but defined structures could be a direction of research. On the other hand, cooperative self-assembly of polypeptide copolymers with a secondary component, such as homopolymers, block copolymers, and nanoparticles, is effective in controlling the structure and function of aggregates in a designed way. For multicomponent self-assembly, systematic studies are needed to explore the self-assembly mechanism and inherent structure of the aggregates. Furthermore, the rigidity and chirality of the polypeptide segments impart distinct self-assembly behaviours, but detailed research on these effects is lacking. For example, the ordering of rigid polypeptide segments from polypeptide copolymers around fibre-like polymer templates can induce the formation of superhelices with identical chirality. The formation mechanism for the identical handedness and the effect of template dimension are important issues to be explored, which should be closely related to the rigidity and chirality characteristics of the polypeptides.

In recent years, great advances in polypeptide drug delivery have been achieved, but there are still critical challenges in the development of polypeptide copolymer assemblies as delivery vehicles. From the viewpoint of delivery applications, the principal demands for delivery systems can be summarized as high loading capacity, high stability during delivery, and controllable release of payloads at target tissues. These demands might be met by using multifunctional polypeptide copolymers (either derived from polypeptides or nonpolypeptide blocks) to construct multi-responsive polypeptide nanocarriers because they have a better release profile than their non-responsive or single-responsive counterparts. Dual- and multi-responsive polypeptide nanocarriers are attracting increasing attention because they offer greater control over drug release.

In addition to the widely studied delivery application, polypeptide assemblies are used as additives to control the biomimetic mineralization of inorganics. Self-assembled aggregates with hydrophilic polypeptides as coronae mimic the essential feature of the folded structure of natural mineralization proteins, which contain both hydrophilic and hydrophobic peptide units and self-assemble (fold) into specific nanostructures. In addition to typical spherical micelles and vesicles, using polypeptide aggregates with non-spherical morphologies, such as cylinders, plates, and rings, to mediate mineralization could create novel structures. Research on polypeptide aggregate-mediated biomimetic mineralization helps elucidate the role that proteins play in biomineralization and solve the problems related to protein-mediated mineralization. Controlling the structure of biominerals to meet the requirements of practical applications should be the core of future work.

The self-assembly of polypeptide copolymers, the drug loading and release of polypeptide aggregate vehicles, and the mineralization of inorganics are complicated physical–chemical processes. Understanding these physical–chemical processes is generally difficult using the experimental methods. Theoretical simulations have thus emerged as a complementary method to investigate these complex physical–chemical processes, because they can provide detailed microscopic information on the dynamic process in a straightforward way. However, insight into these processes by theoretical simulations needs abundant information in a wide range of space scales from nanometers to microns and timescales from picoseconds to seconds. For example, to understand biomineralization, we have to collect the information on crystallization at different scales, which presents a fundamental challenge in simulations. Full atom

models will lead to an expensive computational cost, while current coarse-grained simulations are difficult to represent certain fine structures of the polypeptide, such as the chirality of polypeptide chains. Therefore, effective simulation methods, incorporating the polymer information at atomic/molecular levels and the structural information at microscopic levels, should be developed. Developing multi-scale simulation approaches requires a lot of technical problems to be solved and would be an important topic in future research of polypeptide-based systems. Furthermore, conducting experiments under the guidance of simulation predictions can significantly improve experimental efficiency.

With their inherent advantages, constructing polypeptide-based copolymer self-assemblies for bio-related applications will undoubtedly continue to be an attractive research topic in contemporary macromolecular science. The rapid development in the self-assembly of polypeptide-based copolymers will greatly accelerate the advancement of the fabrication of "smart" delivery systems and diverse mineralization modifiers. However, polypeptide materials are structurally different from natural proteins, which possibly results in altered biocompatibility and enzymatic degradation behaviours. Therefore, evaluating the biocompatibility and biodegradation of these polypeptide materials should be another research focus. We are convinced that, as advanced biomaterials, polypeptide-based assemblies could play an increasingly important role in bio-related applications that is not limited to delivery vehicles and mineralization modifiers.

Abbreviations

AFM	Atomic force microscopy
BD	Brownian dynamics
CCL	Core-crosslinked
DDS	Drug delivery system
DL-PA	Poly(DL-alanine)
DLS	Dynamic light scattering
DMF	*N*,*N*′-Dimethylformamide
DP	Degree of polymerization
DPD	Dissipative particle dynamics
DOX	Doxorubicin
GSH	Glutathione
HEMA	2-Hydroxyethyl methacrylate
L-PA	Poly(L-alanine)
LCST	Lower critical solution temperature
MD	Molecular dynamics
NCA	*N*-Carboxyanhydride
PAA	Polyacrylic acid
PAsp	Polyaspartic acid
PBLA	Poly(β-benzyl L-aspartate)
PBLG	Poly(γ-benzyl L-glutamate)
PDEAm	Poly(*N*,*N*-diethylacrylamide)
PDI	Polydispersity index
PDMAEMA	Poly(2-(dimethylamino)ethyl methacrylate)
PEG	Poly(ethylene glycol)
PEO	Poly(ethylene oxide)
PGMA	Poly(glycidyl methacrylate)
PIAA	Poly(isocyano-L-alanine-L-alanine)
PIAH	Poly(isocyano-L-alanine-L-histidine)
PLeu	Poly(L-leucine)
PLGA	Poly(L-glutamic acid)
PLL	Poly(L-lysine)
PLP	Poly(L-phenylalanine)
PNIPAM	Poly(*N*-isopropyl acrylamides)
PPLG	Poly(γ-propargyl L-glutamate)
PPO	Poly(propylene oxide)
PS	Polystyrene
PZLys	Poly(ε-carbobenzoxy-L-lysine)/poly(ε-benzyloxycarbonyl-L-lysine)
RAFT	Reversible addition–fragmentation chain transfer
ROP	Ring-opening polymerization
SCFT	Self-consistent field theory
SCL	Shell-crosslinked
SEM	Scanning electron microscopy
SLS	Static light scattering
TEM	Transmission electron microscopy
THF	Tetrahydrofuran

Acknowledgements

This work was supported by the National Natural Science Foundation of China (51303055, 51573049, 21234002, and 21474029) and the National Basic Research Program of China (2012CB933600). Support from Projects of Shanghai municipality (15QA1401400, 15ZZ028, and 13JC1402000) and Fundamental Research Funds for the Central Universities (22A201514001) is also appreciated.

References

1 J. Huang and A. Heise, *Chem. Soc. Rev.*, 2013, **42**, 7373–7390.
2 C. Deng, J. Wu, R. Cheng, F. Meng, H.-A. Klok and Z. Zhong, *Prog. Polym. Sci.*, 2014, **39**, 330–364.
3 H. Lu, J. Wang, Z. Song, L. Yin, Y. Zhang, H. Tang, C. Tu, Y. Lin and J. Cheng, *Chem. Commun.*, 2014, **50**, 139–155.
4 H. Liu, Y. Xiao, H. Xu, Y. Guan, J. Zhang and M. Lang, *Chem. Commun.*, 2015, **51**, 10174–10177.
5 C. Cai, L. Wang and J. Lin, *Chem. Commun.*, 2011, **47**, 11189–11203.
6 C. Meier, Y. Wu, G. Pramanik and T. Weil, *Biomacromolecules*, 2014, **15**, 219–227.
7 L. Zhao, N. Li, K. Wang, C. Shi, L. Zhang and Y. Luan, *Biomaterials*, 2014, **35**, 1284–1301.
8 Z. Song, H. Kim, X. Ba, R. Baumgartner, J. Seok Lee, H. Tang, C. Leal and J. Cheng, *Soft Matter*, 2015, **11**, 4091–4098.
9 L. Wei, C. Cai, J. Lin and T. Chen, *Biomaterials*, 2009, **30**, 2606–2613.
10 Y. Bae and K. Kataoka, *Adv. Drug Delivery Rev.*, 2009, **61**, 768–784.
11 T. J. Deming, *Prog. Polym. Sci.*, 2007, **32**, 858–875.

12 C. He, X. Zhuang, Z. Tang, H. Tian and X. Chen, *Adv. Healthcare Mater.*, 2012, **1**, 48–78.
13 X. Guo, L. Liu, W. Wang, J. Zhang, Y. Wang and S.-H. Yu, *CrystEngComm*, 2011, **13**, 2054–2061.
14 W. Zhu, C. Cai, J. Lin, L. Wang, L. Chen and Z. Zhuang, *Chem. Commun.*, 2012, **48**, 8544–8546.
15 C.-L. Chen and N. L. Rosi, *Angew. Chem., Int. Ed.*, 2010, **49**, 1924–1942.
16 C. Feng, Y. Li, D. Yang, J. Hu, X. Zhang and X. Huang, *Chem. Soc. Rev.*, 2011, **40**, 1282–1295.
17 Y. Mai and A. Eisenberg, *Chem. Soc. Rev.*, 2012, **41**, 5969–5985.
18 L. Li, K. Raghupathi, C. Song, P. Prasad and S. Thayumanavan, *Chem. Commun.*, 2014, **50**, 13417–13432.
19 H. Xu, D. Chen, S. Wang, Y. Zhou, J. Su, W. Zhang and X. Zhang, *Philos. Trans. R. Soc., A*, 2013, **371**, 20120305.
20 L. Wang, J. Lin and X. Zhang, *Polymer*, 2013, **54**, 3427–3442.
21 Y. Liu, B. Liu and Z. Nie, *Nano Today*, 2015, **10**, 278–300.
22 A. O. Moughton, M. A. Hillmyer and T. P. Lodge, *Macromolecules*, 2012, **45**, 2–19.
23 E. Betthausen, C. Hanske, M. Müller, A. Fery, F. H. Schacher, A. H. E. Müller and D. J. Pochan, *Macromolecules*, 2014, **47**, 1672–1683.
24 M. A. Hillmyer, *Science*, 2007, **317**, 604–605.
25 M. Lee, B.-K. Cho and W.-C. Zin, *Chem. Rev.*, 2001, **101**, 3869–3892.
26 K. T. Kim, C. Park, G. W. M. Vandermeulen, D. A. Rider, C. Kim, M. A. Winnik and I. Manners, *Angew. Chem., Int. Ed.*, 2005, **44**, 7964–7968.
27 S. Lin, N. Numasawa, T. Nose and J. Lin, *Macromolecules*, 2007, **40**, 1684–1692.
28 W. Ding, S. Lin, J. Lin and L. Zhang, *J. Phys. Chem. B*, 2008, **112**, 776–783.
29 X. Lin, X. He, C. Hu, Y. Chen, Y. Mai and S. Lin, *Polym. Chem.*, 2016, **7**, 2815–2820.
30 A. Carlsen and S. Lecommandoux, *Curr. Opin. Colloid Interface Sci.*, 2009, **14**, 329–339.
31 J. A. Hanson, Z. Li and T. J. Deming, *Macromolecules*, 2010, **43**, 6268–6269.
32 H. Matsui, M. Ueda, A. Makino and S. Kimura, *Chem. Commun.*, 2012, **48**, 6181–6183.
33 G. S. Kwon and K. Kataoka, *Adv. Drug Delivery Rev.*, 2012, **64**, 237–245.
34 R. Gupta, J. Shea, C. Scaife, A. Shurlygina and N. Rapoport, *J. Controlled Release*, 2015, **212**, 70–77.
35 T. M. Allen and P. R. Cullis, *Science*, 2004, **303**, 1818–1822.
36 H. Xu, Q. Yao, C. Cai, J. Gou, Y. Zhang, H. Zhong and X. Tang, *J. Controlled Release*, 2015, **199**, 84–97.
37 J. Deng, N. Gao, Y. Wang, H. Yi, S. Fang, Y. Ma and L. Cai, *Biomacromolecules*, 2012, **13**, 3795–3804.
38 R. P. Johnson, Y.-I. Jeong, E. Choi, C.-W. Chung, D. H. Kang, S.-O. Oh, H. Suh and I. Kim, *Adv. Funct. Mater.*, 2012, **22**, 1058–1068.
39 L. Wei, J. Lin, C. Cai, Z. Fang and W. Fu, *Eur. J. Pharm. Biopharm.*, 2011, **78**, 346–354.
40 Y. Bae, S. Fukushima, A. Harada and K. Kataoka, *Angew. Chem., Int. Ed.*, 2003, **42**, 4640–4643.
41 S. J. Shirbin, K. Ladewig, Q. Fu, M. Klimak, X. Zhang, W. Duan and G. G. Qiao, *Biomacromolecules*, 2015, **16**, 2463–2474.
42 E. M. Mastria, M. Chen, J. R. McDaniel, X. Li, J. Hyun, M. W. Dewhirst and A. Chilkoti, *J. Controlled Release*, 2015, **208**, 52–58.
43 M. Xu, J. Qian, A. Suo, T. Liu, X. Liu and H. Wang, *Polym. Chem.*, 2015, **6**, 2445–2456.
44 S. Kashyap and M. Jayakannan, *J. Mater. Chem. B*, 2014, **2**, 4142–4152.
45 S. Kim and C. B. Park, *Adv. Funct. Mater.*, 2013, **23**, 10–25.
46 F. Nudelman and N. Sommerdijk, *Angew. Chem., Int. Ed.*, 2012, **51**, 6582–6596.
47 P. C. Nagajyothi, M. Pandurangan, T. V. M. Sreekanth and J. Shim, *J. Photochem. Photobiol., B*, 2016, **156**, 29–34.
48 F. Jones and M. I. Ogden, *CrystEngComm*, 2010, **12**, 1016–1023.
49 D. Noda, Y. Arai, D. Souma, H. Nagashima and R.-H. Jin, *Chem. Commun.*, 2014, **50**, 10793–10796.
50 M. A. Bewernitz, D. Gebauer, J. Long, H. Colfen and L. B. Gower, *Faraday Discuss.*, 2012, **159**, 291–312.
51 X. Guo, A. Xu and S. Yu, *Cryst. Growth Des.*, 2008, **8**, 1233–1242.
52 T. Sugawara, Y. Suwa, K. Ohkawa and H. Yamamoto, *Macromol. Rapid Commun.*, 2003, **24**, 847–851.
53 J. N. Cha, G. D. Stucky, D. E. Morse and T. J. Deming, *Nature*, 2000, **403**, 289–292.
54 Y. Yao, D. Wang, L. Han and S. Che, *Chem. – Eur. J.*, 2013, **19**, 15489–15492.
55 W. Zhu, J. Lin, C. Cai and Y. Lu, *J. Mater. Chem. B*, 2013, **1**, 841–849.
56 H. Cao, J. Yao and Z. Shao, *J. Solid State Chem.*, 2013, **199**, 338–343.
57 K. Bleek and A. Taubert, *Acta Biomater.*, 2013, **9**, 6283–6321.
58 F. Gai, T. Zhou, Y. Liu and Q. Huo, *J. Mater. Chem. A*, 2015, **3**, 2120–2127.
59 A. S. Schenk, H. Zope, Y.-Y. Kim, A. Kros, N. A. J. M. Sommerdijk and F. C. Meldrum, *Faraday Discuss.*, 2012, **159**, 327–344.
60 L. E. Euliss, M. H. Bartl and G. D. Stucky, *J. Cryst. Growth*, 2006, **286**, 424–430.
61 W. Zhu, J. Lin and C. Cai, *J. Mater. Chem.*, 2012, **22**, 3939–3947.
62 J. D. Hartgerink, E. Beniash and S. I. Stupp, *Science*, 2001, **294**, 1684–1688.
63 X.-H. Guo, S.-H. Yu and G.-B. Cai, *Angew. Chem., Int. Ed.*, 2006, **45**, 3977–3981.
64 Y. Lu, C. Cai, J. Lin and Q. Zhuang, *J. Mater. Chem. B*, 2016, **4**, 3721–3732.
65 W. Kong, W. Jiang, Y. Zhu and B. Li, *Langmuir*, 2012, **28**, 11714–11724.
66 Y.-L. Lin, H.-Y. Chang, Y.-J. Sheng and H.-K. Tsao, *Soft Matter*, 2014, **10**, 1500–1511.

67 A. K. Omar, B. Hanson, R. T. Haws, Z. Hu, D. A. Vanden Bout, P. J. Rossky and V. Ganesan, *J. Phys. Chem. B*, 2015, **119**, 330–337.
68 J. H. Harding, D. M. Duffy, M. L. Sushko, P. M. Rodger, D. Quigley and J. A. Elliott, *Chem. Rev.*, 2008, **108**, 4823–4854.
69 X. Guo, L. Zhang, Z. Wu and Y. Qian, *Macromolecules*, 2010, **43**, 7839–7844.
70 J. L. Woodhead and C. K. Hall, *Macromolecules*, 2011, **44**, 5443–5451.
71 S. M. Loverde, M. L. Klein and D. E. Discher, *Adv. Mater.*, 2012, **24**, 3823–3830.
72 Y. Zhou, S. Song, X.-P. Long, C.-Y. Zhang and Y.-M. Chen, *Macromol. Theory Simul.*, 2014, **23**, 490–499.
73 Z. Luo and J. Jiang, *J. Controlled Release*, 2012, **162**, 185–193.
74 N. Almora-Barrios and N. H. De Leeuw, *Cryst. Growth Des.*, 2012, **12**, 756–763.
75 Y. Yang, Q. Cui and N. Sahai, *Langmuir*, 2010, **26**, 9848–9859.
76 Y. Han, H. Yu, H. Du and W. Jiang, *J. Am. Chem. Soc.*, 2010, **132**, 1144–1150.
77 L. Zheng, Y. Yang, X. Guo, Y. Sun, Y. Qian and L. Zhang, *J. Colloid Interface Sci.*, 2011, **363**, 114–121.
78 J. Xu, Y. Han, J. Cui and W. Jiang, *Langmuir*, 2013, **29**, 10383–10392.
79 L. Chen, T. Jiang, C. Cai, L. Wang, J. Lin and X. Cao, *Adv. Healthcare Mater.*, 2014, **3**, 1508–1517.
80 M. Ramezanpour, S. S. W. Leung, K. H. Delgado-Magnero, B. Y. M. Bashe, J. Thewalt and D. P. Tieleman, *Biochim. Biophys. Acta*, 2016, **1858**, 1688–1709.
81 J. C. Johnson, L. S. T. J. Korley and M. Tsige, *J. Phys. Chem. B*, 2014, **118**, 13718–13728.
82 J. W. Singer, A. O. Yazaydin, R. J. Kirkpatrick and G. M. Bowers, *Chem. Mater.*, 2012, **24**, 1828–1836.
83 J. J. L. M. Cornelissen, M. Fischer, N. A. J. M. Sommerdijk and R. J. M. Nolte, *Science*, 1998, **280**, 1427–1430.
84 I. Ozcan, F. Segura-Sánchez, K. Bouchemal, M. Sezak, O. Ozer, T. Güneri and G. Ponchel, *Int. J. Nanomed.*, 2010, **5**, 1103–1111.
85 M. E. Martínez-Barbosa, S. Cammas-Marion, L. Bouteiller, C. Vauthier and G. Ponchel, *Bioconjugate Chem.*, 2009, **20**, 1490–1496.
86 C. Cai, J. Lin, T. Chen, X.-S. Wang and S. Lin, *Chem. Commun.*, 2009, 2709–2711.
87 C. Cai, Y. Li, J. Lin, L. Wang, S. Lin, X.-S. Wang and T. Jiang, *Angew. Chem., Int. Ed.*, 2013, **52**, 7732–7736.
88 O. F. Mutaf, A. Kishimura, Y. Mochida, A. Kim and K. Kataoka, *Macromol. Rapid Commun.*, 2015, **36**, 1958–1964.
89 X. Xu, H. Yuan, J. Chang, B. He and Z. Gu, *Angew. Chem., Int. Ed.*, 2012, **51**, 3130–3133.
90 S. Abraham, C.-S. Ha, C. A. Batt and I. Kim, *J. Polym. Sci., Part A: Polym. Chem.*, 2007, **45**, 3570–3579.
91 N. Sharma, A. Top, K. L. Kiick and D. J. Pochan, *Angew. Chem., Int. Ed.*, 2009, **48**, 7078–7082.
92 R. Wang, N. Xu, F.-S. Du and Z.-C. Li, *Chem. Commun.*, 2010, **46**, 3902–3904.
93 S. Jain and F. S. Bates, *Science*, 2003, **300**, 460–464.
94 P. Bhargava, Y. Tu, J. X. Zheng, H. Xiong, R. P. Quirk and S. Z. D. Cheng, *J. Am. Chem. Soc.*, 2007, **129**, 1113–1121.
95 C. Liu, L. Yao, H. Wang, Z. R. Phua, X. Song and H. Chen, *Small*, 2014, **10**, 1332–1340.
96 C. Cai, J. Lin, Z. Zhuang and W. Zhu, *Adv. Polym. Sci.*, 2013, **259**, 159–200.
97 A. Kros, W. Jesse, G. A. Metselaar and J. J. L. M. Cornelissen, *Angew. Chem., Int. Ed.*, 2005, **44**, 4349–4352.
98 J. Huang, C. Bonduelle, J. Thévenot, S. Lecommandoux and A. Heise, *J. Am. Chem. Soc.*, 2012, **134**, 119–122.
99 Z. Zhuang, C. Cai, T. Jiang, J. Lin and C. Yang, *Polymer*, 2014, **55**, 602–610.
100 C. Cai, L. Zhang, J. Lin and L. Wang, *J. Phys. Chem. B*, 2008, **112**, 12666–12673.
101 C.-J. Huang and F.-C. Chang, *Macromolecules*, 2008, **41**, 7041–7052.
102 J. G. Ray, S. S. Naik, E. A. Hoff, A. J. Johnson, J. T. Ly, C. P. Easterling, D. L. Patton and D. A. Savin, *Macromol. Rapid Commun.*, 2012, **33**, 819–826.
103 X. Zhang, S. Monge, M. In, O. Giani and J.-J. Robin, *Soft Matter*, 2013, **9**, 1301–1309.
104 J. Shen, C. Chen, W. Fu, L. Shi and Z. Li, *Langmuir*, 2013, **29**, 6271–6278.
105 L. Wang, J. Lin and L. Zhang, *Macromolecules*, 2010, **43**, 1602–1609.
106 M.-T. Popescu, M. Korogiannaki, K. Marikou and C. Tsitsilianis, *Polymer*, 2014, **55**, 2943–2951.
107 M.-J. Wang, H. Wang, S.-C. Chen, C. Chen and Y. Liu, *Langmuir*, 2015, **31**, 6971–6980.
108 Y. Huang, Y. Mai, X. Yang, U. Beser, J. Liu, F. Zhang, D. Yan, K. Müllen and X. Feng, *J. Am. Chem. Soc.*, 2015, **137**, 11602–11605.
109 L. Wang, T. Jiang and J. Lin, *RSC Adv.*, 2013, **3**, 19481–19491.
110 A. Kikuchi and T. Nose, *Macromolecules*, 1997, **30**, 896–902.
111 W. Wang, W. Wang, X. Lu, S. Bobade, J. Chen, N.-G. Kang, Q. Zhang and J. Mays, *Macromolecules*, 2014, **47**, 7284–7295.
112 L. Zhang, J. Lin and S. Lin, *J. Phys. Chem. B*, 2007, **111**, 9209–9217.
113 S. Zhai, X. Song, C. Feng, X. Jiang, Y. Li, G. Lu and X. Huang, *Polym. Chem.*, 2013, **4**, 4134–4144.
114 B.-Y. Chen, Y.-F. Huang, Y.-C. Huang, T.-C. Wen and J.-S. Jan, *ACS Macro Lett.*, 2014, **3**, 220–223.
115 A. C. Engler, H. Lee and P. T. Hammond, *Angew. Chem., Int. Ed.*, 2009, **48**, 9334–9338.
116 H. Song, R. Li, S. Duan, B. Yu, H. Zhao, D. Chen and F. Xu, *Nanoscale*, 2015, **7**, 5803–5814.
117 P.-C. Li, Y.-C. Lin, M. Chen and S.-W. Kuo, *Soft Matter*, 2013, **9**, 11257–11269.
118 C. Cai, J. Lin, T. Chen and X. Tian, *Langmuir*, 2010, **26**, 2791–2797.
119 J. Lin, G. Zhu, X. Zhu, S. Lin, T. Nose and W. Ding, *Polymer*, 2008, **49**, 1132–1136.
120 D. Tang, J. Lin, S. Lin, S. Zhang, T. Chen and X. Tian, *Macromol. Rapid Commun.*, 2004, **25**, 1241–1246.

121 A. Dag, H. Sahin, H. Durmaz, G. Hizal and U. Tunca, *J. Polym. Sci., Part A: Polym. Chem.*, 2011, **49**, 886–892.
122 S. Ito, S. Senda, T. Ishizone and A. Hirao, *Polym. Chem.*, 2016, **7**, 2078–2086.
123 C. Zhao, P. He, C. Xiao, X. Gao, X. Zhuang and X. Chen, *J. Colloid Interface Sci.*, 2011, **359**, 436–442.
124 H. Luo, J. L. Santos and M. Herrera-Alonso, *Chem. Commun.*, 2014, **50**, 536–538.
125 A. P. Martinez, Z. Cui, C. Hire, T. A. P. Seery and D. H. Adamson, *Macromolecules*, 2015, **48**, 4250–4255.
126 X. Zhang, L. Zhao, J. Yang and J. Yang, *RSC Adv.*, 2016, **6**, 21486–21496.
127 Y. Shi, W. Zhu, D. Yao, M. Long, B. Peng, K. Zhang and Y. Chen, *ACS Macro Lett.*, 2014, **3**, 70–73.
128 C. Cai, W. Zhu, T. Chen, J. Lin and X. Tian, *J. Polym. Sci., Part A: Polym. Chem.*, 2009, **47**, 5967–5978.
129 A. J. Rhodes and T. J. Deming, *J. Am. Chem. Soc.*, 2012, **134**, 19463–19467.
130 J. Wang, H. Lu, Y. Ren, Y. Zhang, M. Morton, J. Cheng and Y. Lin, *Macromolecules*, 2011, **44**, 8699–8708.
131 Z. Wei, S. Zhu and H. Zhao, *Polym. Chem.*, 2015, **6**, 1316–1324.
132 Y. Tang, L. Liu, J. Wu and J. Duan, *J. Colloid Interface Sci.*, 2013, **397**, 24–31.
133 M. Scholl, Z. Kadlecova and H.-A. Klok, *Prog. Polym. Sci.*, 2009, **34**, 24–61.
134 A. Karatzas, H. Iatrou, N. Hadjichristidis, K. Inoue, K. Sugiyama and A. Hirao, *Biomacromolecules*, 2008, **9**, 2072–2080.
135 M. A. Mintzer and M. W. Grinstaff, *Chem. Soc. Rev.*, 2011, **40**, 173–190.
136 X. Xu, C. Li, H. Li, R. Liu, C. Jiang, Y. Wu, B. He and Z. Gu, *Sci. China: Chem.*, 2011, **54**, 326–333.
137 L. Chen, T. Chen, W. Fang, Y. Wen, S. Lin, J. Lin and C. Cai, *Biomacromolecules*, 2013, **14**, 4320–4330.
138 C. Bonduelle, S. Mazzaferro, J. Huang, O. Lambert, A. Heise and S. Lecommandoux, *Faraday Discuss.*, 2013, **166**, 137–150.
139 Y. Zhou and D. Yan, *Chem. Commun.*, 2009, 1172–1188.
140 X. Chang and C. Dong, *Biomacromolecules*, 2013, **14**, 3329–3337.
141 J. M Berg, J. L Tymoczko and L. Stryer, *Biochemistry*, W. H. Freeman, New York, 5th edn, 2002, ISBN-10: 0-7167-3051-0.
142 H. Lodish, A. Berk, S. L. Zipursky, P. Matsudaira, D. Baltimore and J. Darnell, *Molecular Cell Biology*, W. H. Freeman, New York, 4th edn, 2000, ISBN-10: 0-7167-3136-3.
143 G. Rizis, T. G. M. van de Ven and A. Eisenberg, *ACS Nano*, 2015, **9**, 3627–3640.
144 G. Cambridge, M. J. Gonzalez-Alvarez, G. Guerin, I. Manners and M. A. Winnik, *Macromolecules*, 2015, **48**, 707–716.
145 J. F. Reuther, D. A. Siriwardane, R. Campos and B. M. Novak, *Macromolecules*, 2015, **48**, 6890–6899.
146 S. Lin, Y. Wang, C. Cai, Y. Xing, J. Lin, T. Chen and X. He, *Nanotechnology*, 2013, **24**, 085602.
147 S. Wu, L. Wang, A. Kroeger, Y. Wu, Q. Zhang and C. Bubeck, *Soft Matter*, 2011, **7**, 11535–11545.
148 Y. Li, T. Jiang, S. Lin, J. Lin, C. Cai and X. Zhu, *Sci. Rep.*, 2015, **5**, 10137.
149 R.-M. Ho, Y.-W. Chiang, S.-C. Lin and C.-K. Chen, *Prog. Polym. Sci.*, 2011, **36**, 376–453.
150 A. E. Rowan and R. J. M. Nolte, *Angew. Chem., Int. Ed.*, 1998, **37**, 63–68.
151 Y. Wang, J. Xu, Y. Wang and H. Chen, *Chem. Soc. Rev.*, 2013, **42**, 2930–2962.
152 M. Liu, L. Zhang and T. Wang, *Chem. Rev.*, 2015, **115**, 7304–7397.
153 A. C. Bloomer, J. N. Champness, G. Bricogne, R. Staden and A. Klug, *Nature*, 1978, **276**, 362–368.
154 A. Klug, *Philos. Trans. R. Soc. London, Ser. B*, 1999, **354**, 531–535.
155 L. Chen, T. Jiang, J. Lin and C. Cai, *Langmuir*, 2013, **29**, 8417–8426.
156 L. Jia, A. Petretic, G. Molev, G. Guerin, I. Manners and M. A. Winnik, *ACS Nano*, 2015, **9**, 10673–10685.
157 L. Zhang, L. Wang and J. Lin, *Soft Matter*, 2014, **10**, 6713–6721.
158 C. Cai and J. Lin, *Nat. Chem.*, 2014, **6**, 857–858.
159 Y. Chen, K. Zhang, X. Wang, F. Zhang, J. Zhu, J. W. Mays, K. L. Wooley and D. J. Pochan, *Macromolecules*, 2015, **48**, 5621–5631.
160 D. Li, X. Jia, X. Cao, T. Xu, H. Li, H. Qian and L. Wu, *Macromolecules*, 2015, **48**, 4104–4114.
161 N. Moreno, S. P. Nunes, K.-V. Peinemann and V. M. Calo, *Macromolecules*, 2015, **48**, 8036–8044.
162 Z. Zhuang, X. Zhu, C. Cai, J. Lin and L. Wang, *J. Phys. Chem. B*, 2012, **116**, 10125–10134.
163 A. Harada and K. Kataoka, *Science*, 1999, **283**, 65–67.
164 M. Ueda, A. Makino, T. Imai, J. Sugiyama and S. Kimura, *Soft Matter*, 2011, **7**, 4143–4146.
165 Y. Kang and T. A. Taton, *Angew. Chem., Int. Ed.*, 2005, **44**, 409–412.
166 S. Ma, D. Qi, M. Xiao and R. Wang, *Soft Matter*, 2014, **10**, 9090–9097.
167 R. J. Hickey, A. S. Haynes, J. M. Kikkawa and S.-J. Park, *J. Am. Chem. Soc.*, 2011, **133**, 1517–1525.
168 L. Zhang, J. Lin and S. Lin, *Macromolecules*, 2007, **40**, 5582–5592.
169 C. Cai, L. Wang, J. Lin and X. Zhang, *Langmuir*, 2012, **28**, 4515–4524.
170 C. Yang, Q. Li, C. Cai and J. Lin, *Langmuir*, 2016, **32**, 6917–6927.
171 W. Agut, D. Taton, A. Brulet, O. Sandre and S. Lecommandoux, *Soft Matter*, 2011, **7**, 9744–9750.
172 C. Cai, J. Lin, X. Zhu, S. Gong, X.-S. Wang and L. Wang, *Macromolecules*, 2016, **49**, 15–22.
173 O.-S. Lee, S. I. Stupp and G. C. Schatz, *J. Am. Chem. Soc.*, 2011, **133**, 3677–3683.
174 Y. S. Velichko, S. I. Stupp and M. O. de la Cruz, *J. Phys. Chem. B*, 2008, **112**, 2326–2334.
175 G. M. Grason, *ACS Macro Lett.*, 2015, **4**, 526–532.
176 W. Zhao, T. P. Russell and G. M. Grason, *Phys. Rev. Lett.*, 2014, **110**, 058301.

177 C. R. Boehm and E. M. Terentjev, *Macromolecules*, 2014, **47**, 6086–6094.
178 M. S. Aw, M. Kurian and D. Losic, *Chem. – Eur. J.*, 2013, **19**, 12586–12601.
179 S. Mura, J. Nicolas and P. Couvreur, *Nat. Mater.*, 2013, **12**, 991–1003.
180 R. Thipparaboina, R. B. Chavan, D. Kumar, S. Modugula and N. R. Shastri, *Colloids Surf., B*, 2015, **135**, 291–308.
181 R. Trivedi and U. B. Kompella, *Nanomedicine*, 2010, **5**, 485–505.
182 S. C. Owen, D. P. Y. Chan and M. S. Shoichet, *Nano Today*, 2012, **7**, 53–65.
183 M. Tangsangasaksri, H. Takemoto, M. Naito, Y. Maeda, D. Sueyoshi, H. J. Kim, Y. Miura, J. Ahn, R. Azuma, N. Nishiyama, K. Miyata and K. Kataoka, *Biomacromolecules*, 2016, **17**, 246–255.
184 C. Zheng, M. Zheng, P. Gong, J. Deng, H. Yi, P. Zhang, Y. Zhang, P. Liu, Y. Ma and L. Cai, *Biomaterials*, 2013, **34**, 3431–3438.
185 X. Wang, G. Wu, C. Lu, W. Zhao, Y. Wang, Y. Fan, H. Gao and J. Ma, *Eur. J. Pharm. Sci.*, 2012, **47**, 256–264.
186 M. Li, W. Song, Z. Tang, S. Lv, L. Lin, H. Sun, Q. Li, Y. Yang, H. Hong and X. Chen, *ACS Appl. Mater. Interfaces*, 2013, **5**, 1781–1792.
187 Y.-Y. Li, S.-H. Hua, W. Xiao, H.-Y. Wang, X.-H. Luo, C. Li, S.-X. Cheng, X.-Z. Zhang and R.-X. Zhuo, *J. Mater. Chem.*, 2011, **21**, 3100–3106.
188 P. S. Pramod, R. Shah and M. Jayakannan, *Nanoscale*, 2015, **7**, 6636–6652.
189 X. Yang, J. J. Grailer, I. J. Rowland, A. Javadi, S. A. Hurley, V. Z. Matson, D. A. Steeber and S. Gong, *ACS Nano*, 2010, **4**, 6805–6817.
190 T. Yang, F. Li, H. Zhang, L. Fan, Y. Qiao, G. Tan, H. Zhang and H. Wu, *Polym. Chem.*, 2015, **6**, 1373–1382.
191 Y. Bae, W.-D. Jang, N. Nishiyama, S. Fukushima and K. Kataoka, *Mol. BioSyst.*, 2005, **1**, 242–250.
192 Y. Bae, N. Nishiyama, S. Fukushima, H. Koyama, M. Yasuhiro and K. Kataoka, *Bioconjugate Chem.*, 2005, **16**, 122–130.
193 N. Nishiyama, S. Okazaki, H. Cabral, M. Miyamoto, Y. Kato, Y. Sugiyama, K. Nishio, Y. Matsumura and K. Kataoka, *Cancer Res.*, 2005, **63**, 8977–8983.
194 E. W. Durbin and G. A. Buxton, *Soft Matter*, 2010, **6**, 762–767.
195 G. A. Buxton, *Eur. Phys. J. E: Soft Matter Biol. Phys.*, 2014, **37**, 14.
196 T. Yue and X. Zhang, *Soft Matter*, 2013, **9**, 559–569.
197 Y. Li, X. Zhang and D. Cao, *Nanoscale*, 2015, **7**, 2758–2769.
198 G. Saravanakumar, J. Lee, J. Kim and W. J. Kim, *Chem. Commun.*, 2015, **51**, 9995–9998.
199 N. Kalva, N. Parekh and A. V. Ambade, *Polym. Chem.*, 2015, **6**, 6826–6835.
200 X. Xu, Y. Li, H. Li, R. Liu, M. Sheng, B. He and Z. Gu, *Small*, 2014, **10**, 1133–1140.
201 B. Yang, Y. Lv, J. Zhu, Y. Han, H. Jia, W. Chen, J. Feng, X. Zhang and R. Zhuo, *Acta Biomater.*, 2014, **10**, 3686–3695.
202 H. Yin, H. C. Kang, K. M. Huh and Y. H. Bae, *J. Mater. Chem.*, 2012, **22**, 19168–19178.
203 X. Zhang, D. Chen, S. Ba, J. Zhu, J. Zhang, W. Hong, X. Zhao, H. Hu and M. Qiao, *Biomacromolecules*, 2014, **15**, 4032–4045.
204 J. Lin, J. Zhu, T. Chen, S. Lin, C. Cai, L. Zhang, Y. Zhuang and X.-S. Wang, *Biomaterials*, 2009, **30**, 108–117.
205 Q. N. Bui, Y. Li, M.-S. Jang, D. P. Huynh, J. H. Lee and D. S. Lee, *Macromolecules*, 2015, **48**, 4046–4054.
206 M. S. Shim and Y. J. Kwon, *Biomaterials*, 2010, **31**, 3404–3413.
207 H. Sun, R. Cheng, C. Deng, F. Meng, A. A. Dias, M. Hendriks, J. Feijen and Z. Zhong, *Biomacromolecules*, 2015, **16**, 597–605.
208 V. K. Kotharangannagari, A. Sanchez-Ferrer, J. Ruokolainen and R. Mezzenga, *Macromolecules*, 2011, **44**, 4569–4573.
209 G. Li, L. Shi, R. Ma, Y. An and N. Huang, *Angew. Chem., Int. Ed.*, 2006, **45**, 4959–4962.
210 C. L. Lo, K. M. Lin, C. K. Huang and G. H. Hsiue, *Adv. Funct. Mater.*, 2006, **16**, 2309–2316.
211 A. B. E. Attia, Z. Y. Ong, J. L. Hedrick, P. P. Lee, P. L. R. Ee, P. T. Hammond and Y.-Y. Yang, *Curr. Opin. Colloid Interface Sci.*, 2011, **16**, 182–194.
212 Y. Huang, R. Dong, X. Zhu and D. Yan, *Soft Matter*, 2014, **10**, 6121–6138.
213 S. Son, E. Shin and B.-S. Kim, *Biomacromolecules*, 2014, **15**, 628–634.
214 W. Wang, J. Lin, C. Cai and S. Lin, *Eur. Polym. J.*, 2015, **65**, 112–131.
215 G. Liu and C. Dong, *Biomacromolecules*, 2012, **13**, 1573–1583.
216 W.-H. Jian, T.-W. Yu, C.-J. Chen, W.-C. Huang, H.-C. Chiu and W.-H. Chiang, *Langmuir*, 2015, **31**, 6202–6210.
217 G. Liu, N. Liu, L. Zhou, Y. Su and C. Dong, *Polym. Chem.*, 2015, **6**, 4030–4039.
218 S. Kumar, J.-F. Allard, D. Morris, Y. L. Dory, M. Lepage and Y. Zhao, *J. Mater. Chem.*, 2012, **22**, 7252–7257.
219 S. R. Elizabeth and P. A. Steven, *Chem. Commun.*, 2007, 3021–3035.
220 M. Talelli, M. Barz, C. J. F. Rijcken, F. Kiessling, W. E. Hennink and T. Lammers, *Nano Today*, 2015, **10**, 93–117.
221 Y. Li, W. Du, G. Sun and K. L. Wooley, *Macromolecules*, 2008, **41**, 6605–6607.
222 F. Zhang, M. Elsabahy, S. Zhang, L. Y. Lin, J. Zou and K. L. Wooley, *Nanoscale*, 2013, **5**, 3220–3225.
223 F. Jia, Y. Wang, H. Wang, Q. Jin, T. Cai, Y. Chen and J. Ji, *Polym. Chem.*, 2015, **6**, 2069–2075.
224 H. Xu, F. Meng and Z. Zhong, *J. Mater. Chem.*, 2009, **19**, 4183–4190.
225 J. V. M. Weaver, Y. Tang, S. Liu, P. D. Iddon, R. Grigg, N. C. Billingham, S. P. Armes, R. Hunter and S. P. Rannard, *Angew. Chem., Int. Ed.*, 2004, **43**, 1389–1392.
226 A. N. Koo, H. J. Lee, S. E. Kim, J. H. Chang, C. Park, C. Kim, J. H. Park and S. C. Lee, *Chem. Commun.*, 2008, 6570–6572.
227 J. Dai, S. Lin, D. Cheng, S. Zou and X. Shuai, *Angew. Chem., Int. Ed.*, 2011, **50**, 9404–9408.
228 L. Yan, L. Yang, H. He, X. Hu, Z. Xie, Y. Huang and X. Jing, *Polym. Chem.*, 2012, **3**, 1300–1307.
229 L. Wu, Y. Zou, C. Deng, R. Cheng, F. Meng and Z. Zhong, *Biomaterials*, 2013, **34**, 5262–5272.

230 K. Wang, G.-F. Luo, Y. Liu, C. Li, S.-X. Cheng, R.-X. Zhuo and X.-Z. Zhang, *Polym. Chem.*, 2012, **3**, 1084–1090.
231 E. G. Bellomo, M. D. Wyrsta, L. Pakstis, D. J. Pochan and T. J. Deming, *Nat. Mater.*, 2004, **3**, 244–248.
232 K. Feng, S. Wang, H. Ma and Y. Chen, *J. Pharm. Pharmacol.*, 2013, **65**, 64–71.
233 A. Uesaka, M. Ueda, T. Imai, J. Sugiyama and S. Kimura, *Langmuir*, 2014, **30**, 4273–4279.
234 A. Makino, *Polym. J.*, 2014, **46**, 783–791.
235 P. F. Gu, H. Xu, B. W. Sui, J. X. Gou, L. K. Meng, F. Sun, X. J. Wang, N. Qi, Y. Zhang, H. B. He and X. Tang, *Int. J. Nanomed.*, 2012, **7**, 109–122.
236 J. Ding, C. Li, Y. Zhang, W. Xu, J. Wang and X. Chen, *Acta Biomater.*, 2015, **11**, 346–355.
237 P. K. Ajikumar, S. Vivekanandan, R. Lakshminarayanan, S. D. S. Jois, R. M. Kini and S. Valiyaveettil, *Angew. Chem., Int. Ed.*, 2005, **44**, 5476–5479.
238 A. Schulz, H. Wang, P. van Rijn and A. Boker, *J. Mater. Chem.*, 2011, **21**, 18903–18918.
239 S. Kessel, A. Thomas and H. G. Borner, *Angew. Chem., Int. Ed.*, 2007, **46**, 9023–9026.
240 S. Cavalli, F. Albericio and A. Kros, *Chem. Soc. Rev.*, 2010, **39**, 241–263.
241 C.-L. Chen, J. Qi, J. Tao, R. N. Zuckermann and J. J. DeYoreo, *Sci. Rep.*, 2014, **4**, 6266.
242 H. Cao, G. Q. Lin, J. R. Yao and Z. Z. Shao, *Macromol. Biosci.*, 2013, **13**, 650–659.
243 Y. Politi, J. Mahamid, H. Goldberg, S. Weiner and L. Addadi, *CrystEngComm*, 2007, **9**, 1171–1177.
244 Y. Liu, Y. J. Cui and R. Guo, *Langmuir*, 2012, **28**, 6097–6105.
245 M. J. Olszta, S. Gajjeraman, M. Kaufman and L. B. Gower, *Chem. Mater.*, 2004, **16**, 2355–2362.
246 S. J. Homeijer, M. J. Olszta, R. A. Barrett and L. B. Gower, *J. Cryst. Growth*, 2008, **310**, 2938–2945.
247 H. J. Lee, S. E. Kim, I. K. Kwon, C. Park, C. Kim, J. Yang and S. C. Lee, *Chem. Commun.*, 2010, **46**, 377–379.
248 A. Jain, M. Jochum and C. Peter, *Langmuir*, 2014, **30**, 15486–15495.
249 M. Muthukumar, *J. Chem. Phys.*, 2009, **130**, 161101.
250 L. Lenoci and P. J. Camp, *J. Am. Chem. Soc.*, 2006, **128**, 10111–10117.
251 Y.-Y. Kim, K. Ganesan, P. Yang, A. N. Kulak, S. Borukhin, S. Pechook, L. Ribeiro, R. Kroger, S. J. Eichhorn, S. P. Armes, B. Pokroy and F. C. Meldrum, *Nat. Mater.*, 2011, **10**, 890–896.

